Supporting Information

High Temperature Shape Memory Poly(amide-imide)s with Strong Mechanical Robustness

Xingfeng Lei,[a,b*] Guo Xiong,[a,b] Yuyang Xiao,[a,b] Tianhao Huang,[a,b] Xiangze Xin,[a,b] Shuyu Xue,[a,b] Qiuyu Zhang[a,b*]

[a]School of Chemistry and Chemical Engineering, Key Laboratory of Special Functional and Smart Polymer Materials of Ministry of Industry and Information Technology, Northwestern Polytechnical University, Xi'an, Shaanxi, 710072, P. R. China.

[b]School of Chemistry and Chemical Engineering, Key Laboratory of Material Physics and Chemistry under Extraordinary Conditions of Ministry of Education, Northwestern Polytechnical University, Xi'an, Shaanxi, 710072, P. R. China.

[*]Corresponding Authors, E-mail: leifeng@nwpu.edu.cn, qyzhang@nwpu.edu.cn; Fax/Tel: +86-029-88431653.

Digital images of the as-synthesized diamine monomers

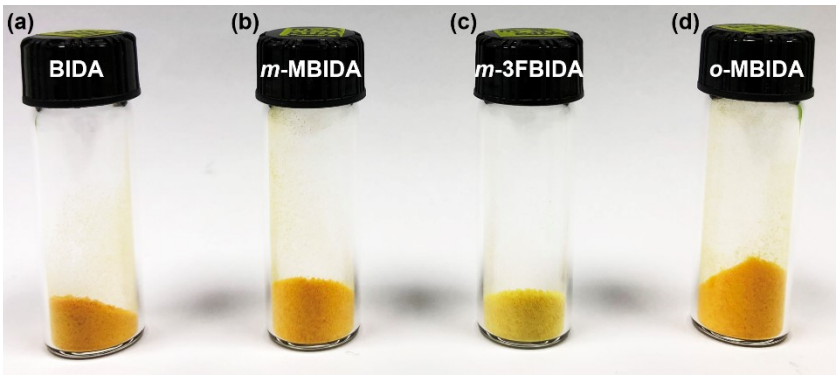

Figure S1. Digital image for the prepared amine-terminated bisimide monomers in glass vials: (a) BIDA, (b) *m*-MBIDA, (c) *m*-3FBIDA, (d) *o*-MBIDA

Additional Characterizations

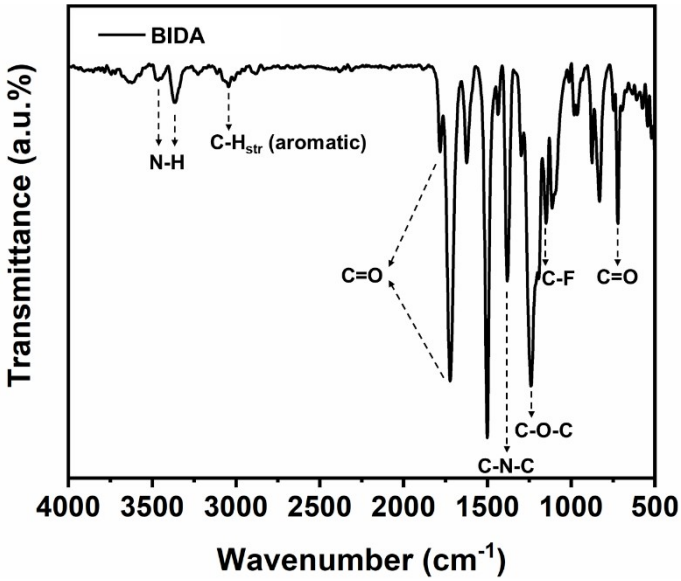

Figure S2. FT-IR spectrum of BIDA monomer

Taking **BIDA** as an example to analyze the molecular structures of the diamine monomers. **Figure S3** gives the ^{1}H-NMR spectra of **BIDA** in DMSO-d_6. As indicated, the peaks in the range of 8.17-7.72 ppm are assigned to the hydrogens of **6FDA** moiety, and the peaks at around 7.40-6.60 ppm are ascribed to the aromatic protons of **ODA** moiety. The singlet peak locating at 5.05 ppm corresponds to primary amino proton. ^{13}C-NMR spectrum of **BIDA** in $CDCl_3$ shown in **Figure S4** displays characteristic carbon signals including imide carbonyl (~166.2 ppm), aromatic carbons (~116.2-159.1 ppm, containing carbons in **ODA** and **6FDA** moieties) and the quaternary carbon connecting with two trifluoromethyl groups of **6FDA** (~65 ppm). The trifluoromethyl carbon signal locates at ca. 124.1 ppm and any signal of poly(amic acid) appearing at ~175 ppm is absent, and the proton integral is consistent with the theoretical composition of **BIDA** molecule, testifying to the successful preparation of **BIDA** diamine monomer.

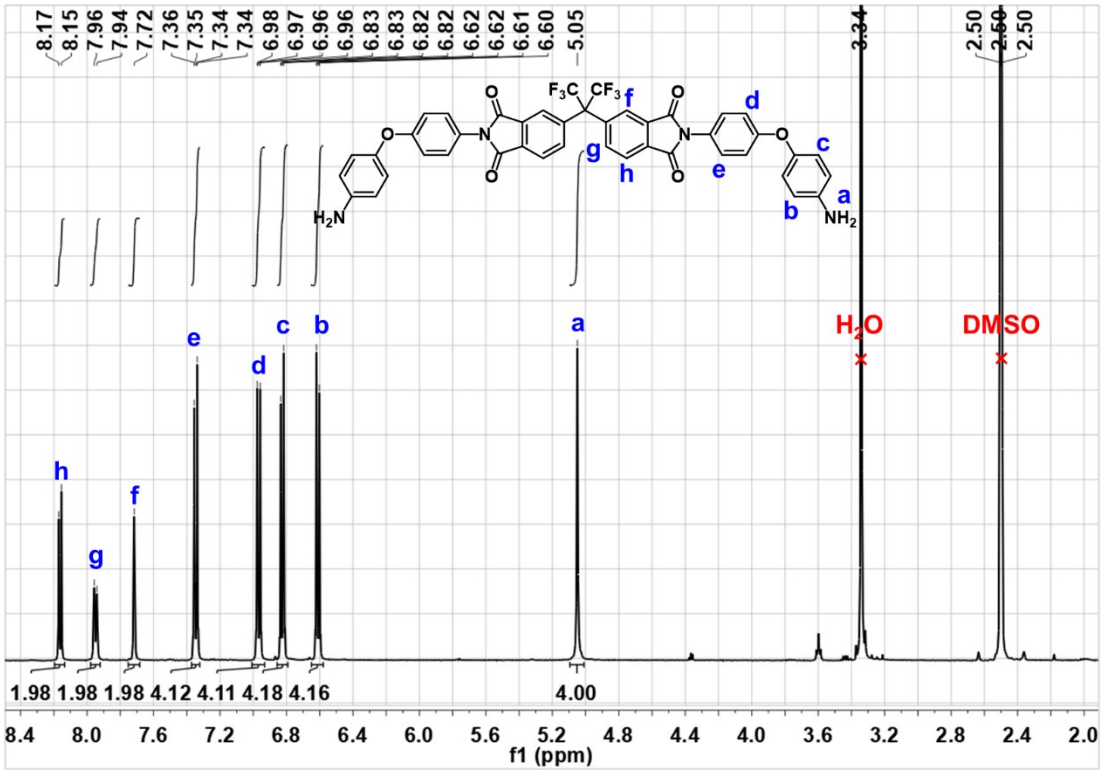

Figure S3. [1]H-NMR spectrum of BIDA monomer in DMSO-d_6

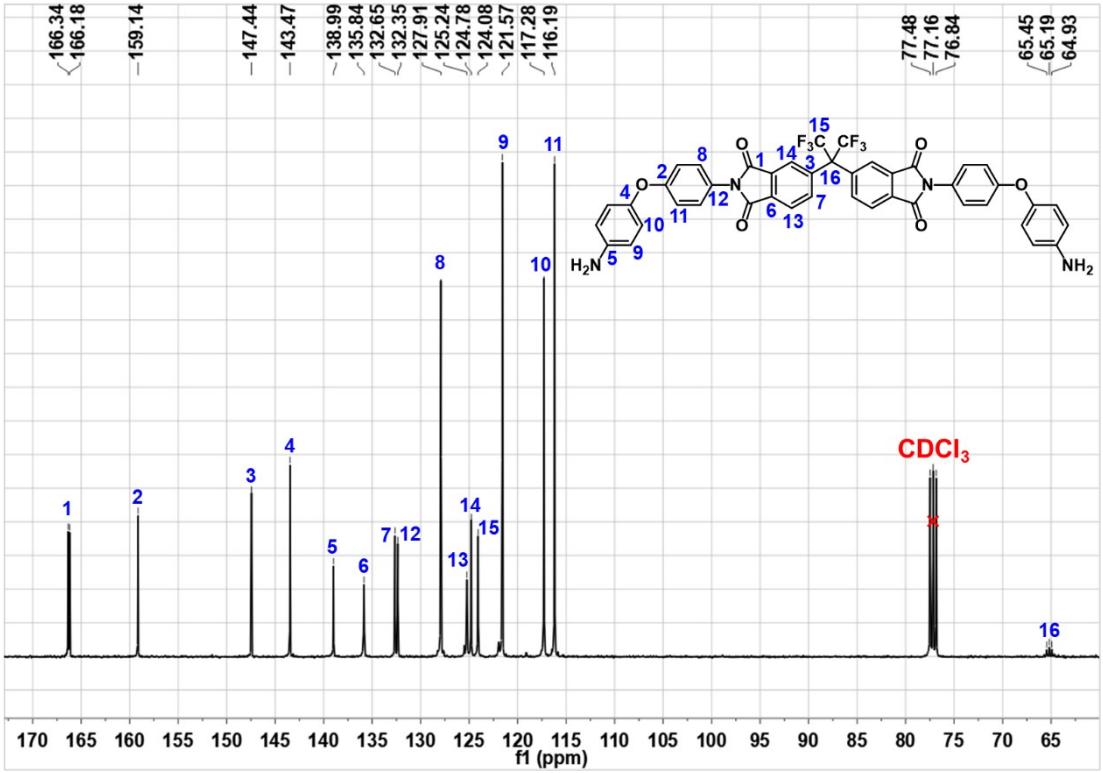

Figure S4. [13]C-NMR spectrum of BIDA monomer in $CDCl_3$

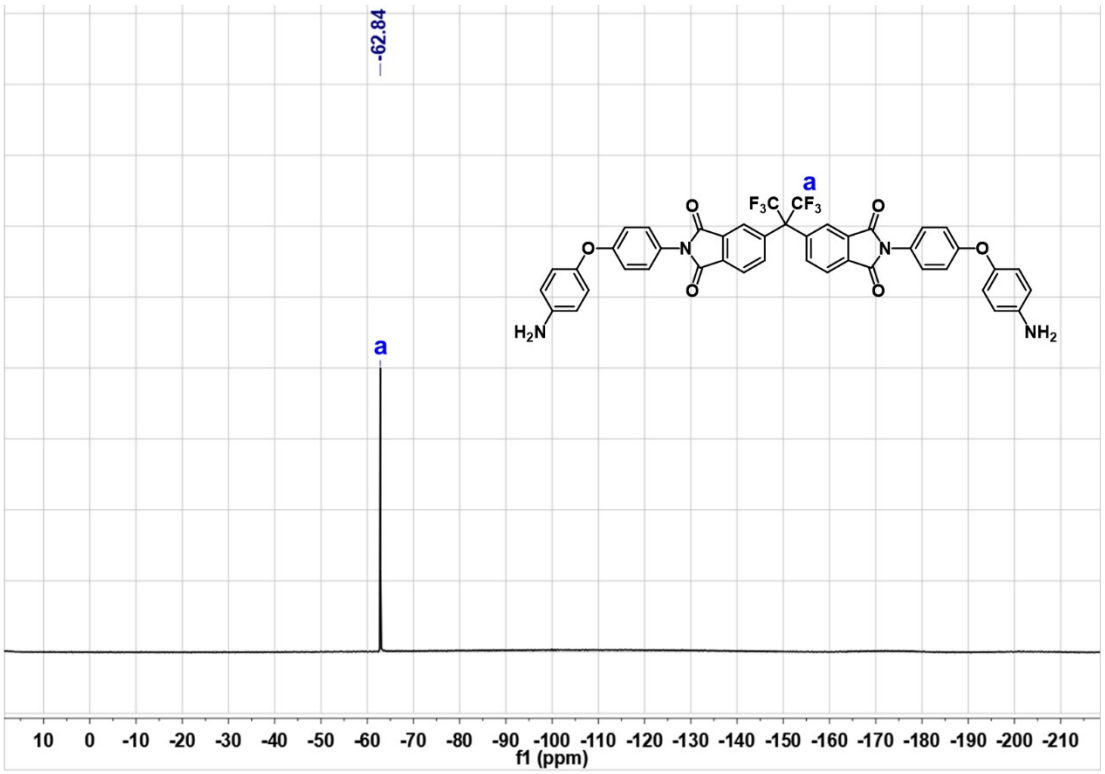

Figure S5. ^{19}F-NMR spectrum of BIDA monomer in DMSO-d_6

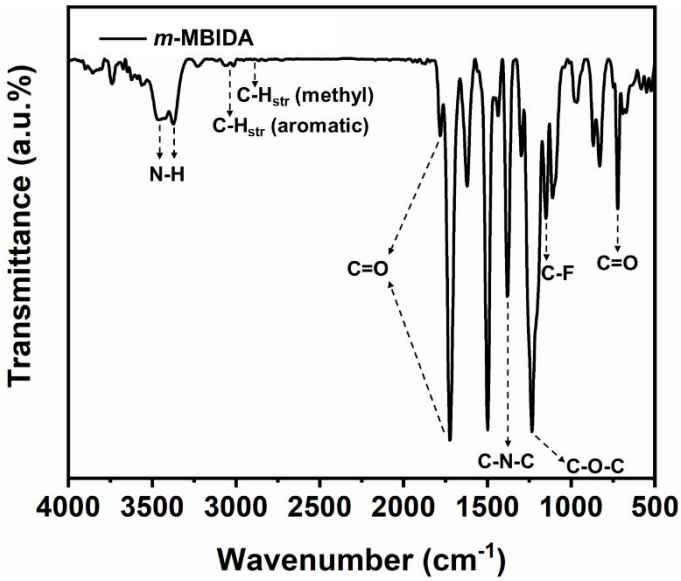

Figure S6. FT-IR spectrum of *m*-MBIDA monomer

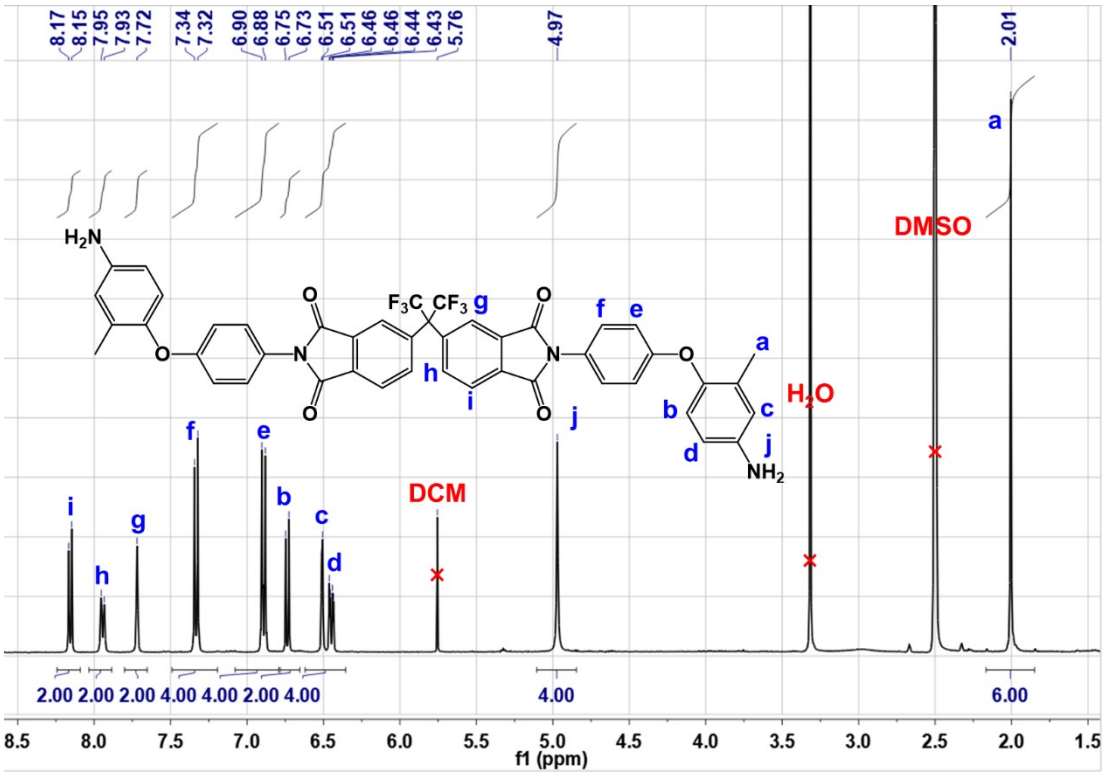

Figure S7. ^{1}H-NMR spectrum of *m*-MBIDA monomer in DMSO-d_6

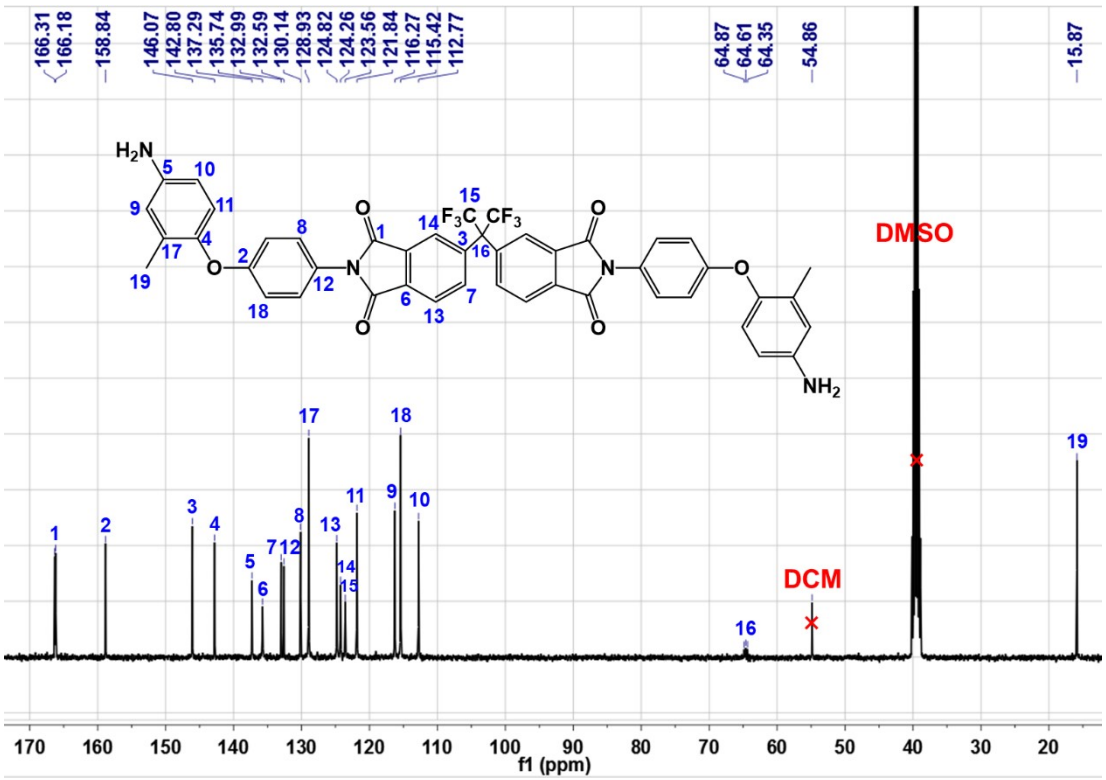

Figure S8. ^{13}C-NMR spectrum of *m*-MBIDA monomer in DMSO-d_6

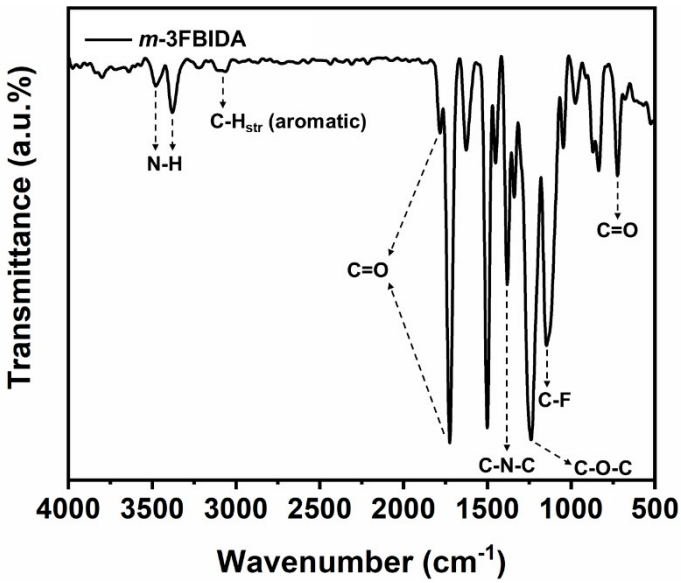

Figure S9. FT-IR spectrum of *m*-3FBIDA monomer

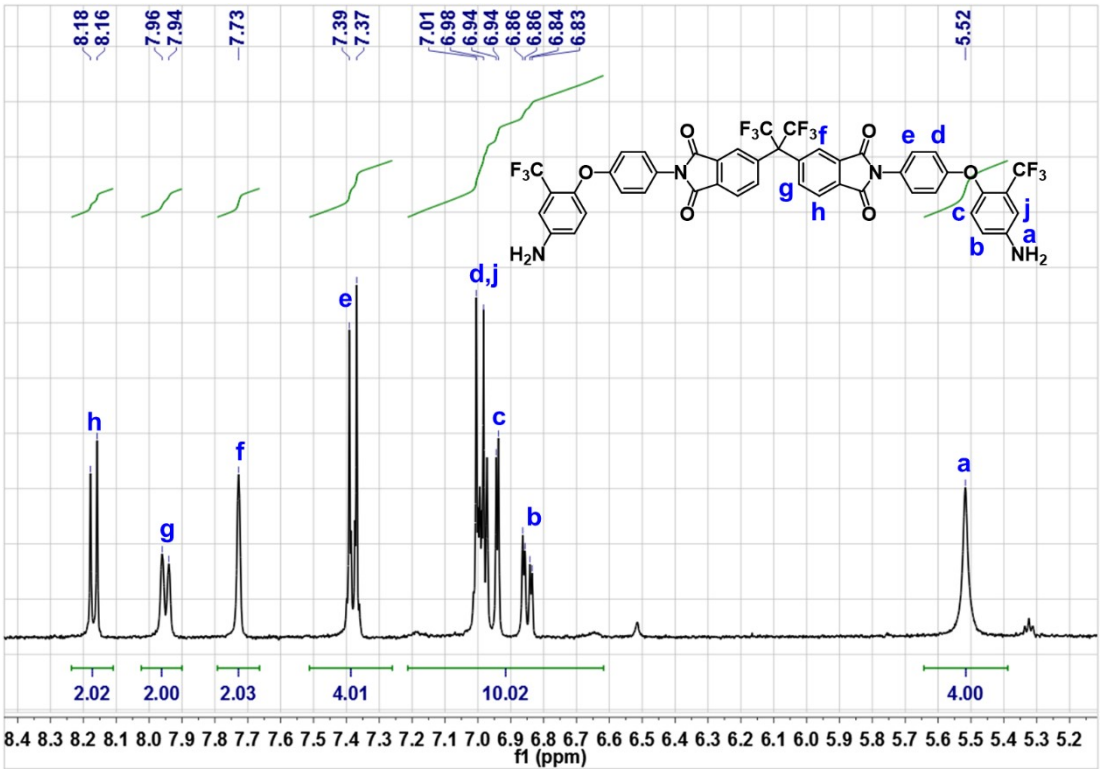

Figure S10. ^{1}H-NMR spectrum of *m*-3FBIDA monomer in DMSO-d_6

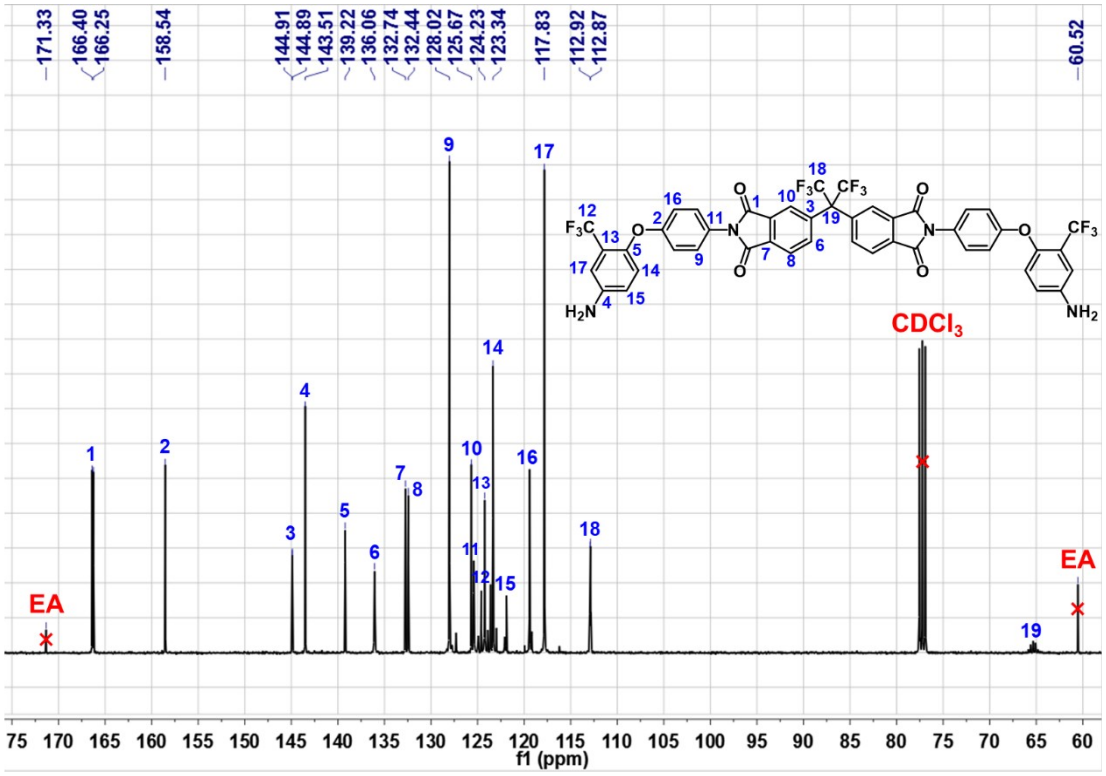

Figure S11. ^{13}C-NMR spectrum of *m*-3FBIDA monomer in $CDCl_3$

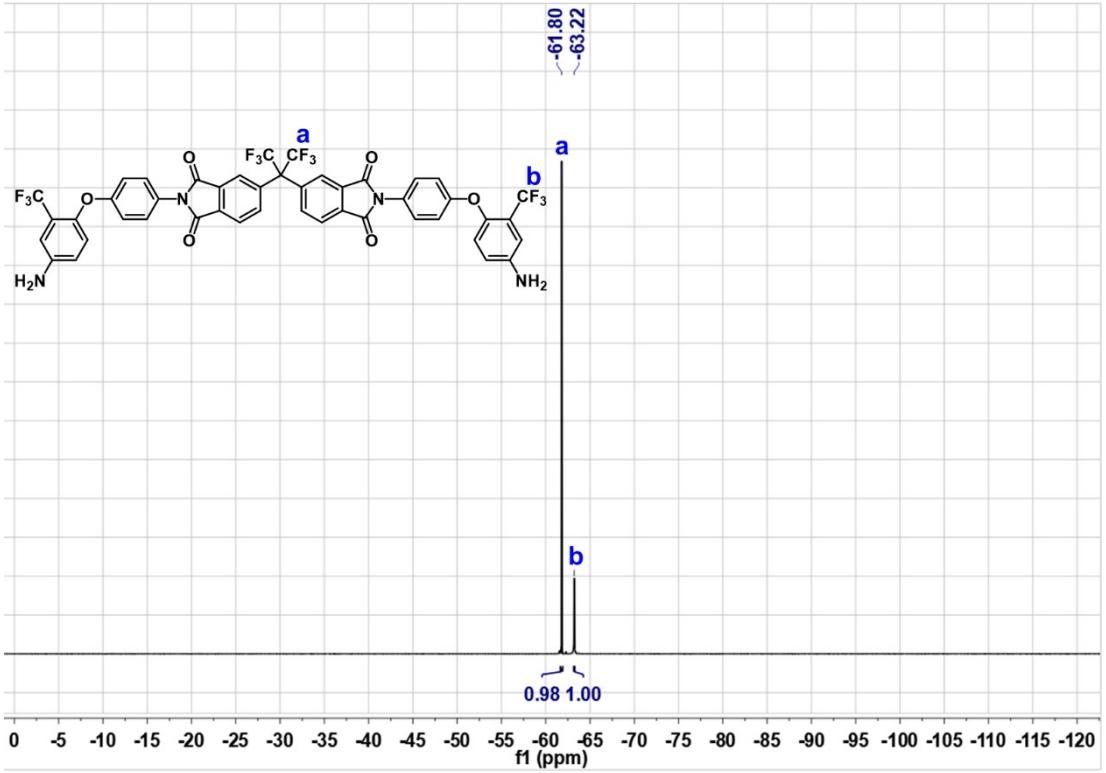

Figure S12. ^{19}F-NMR spectrum of *m*-3FBIDA monomer in DMSO-d_6

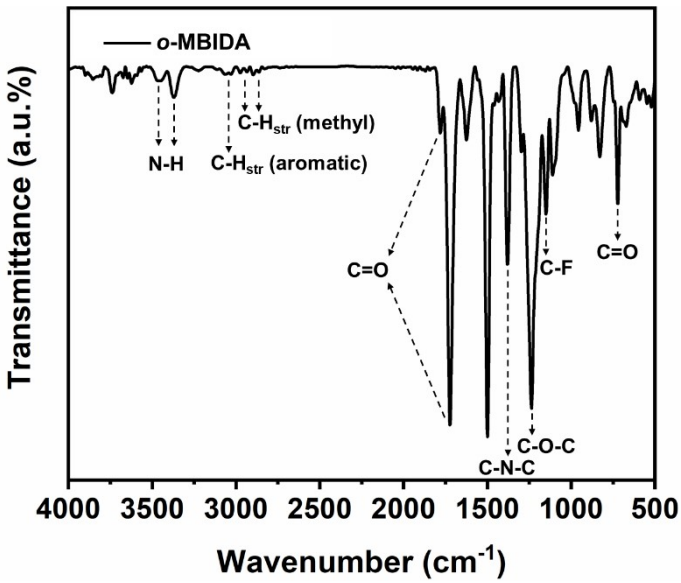

Figure S13. FT-IR spectrum of *o*-MBIDA monomer

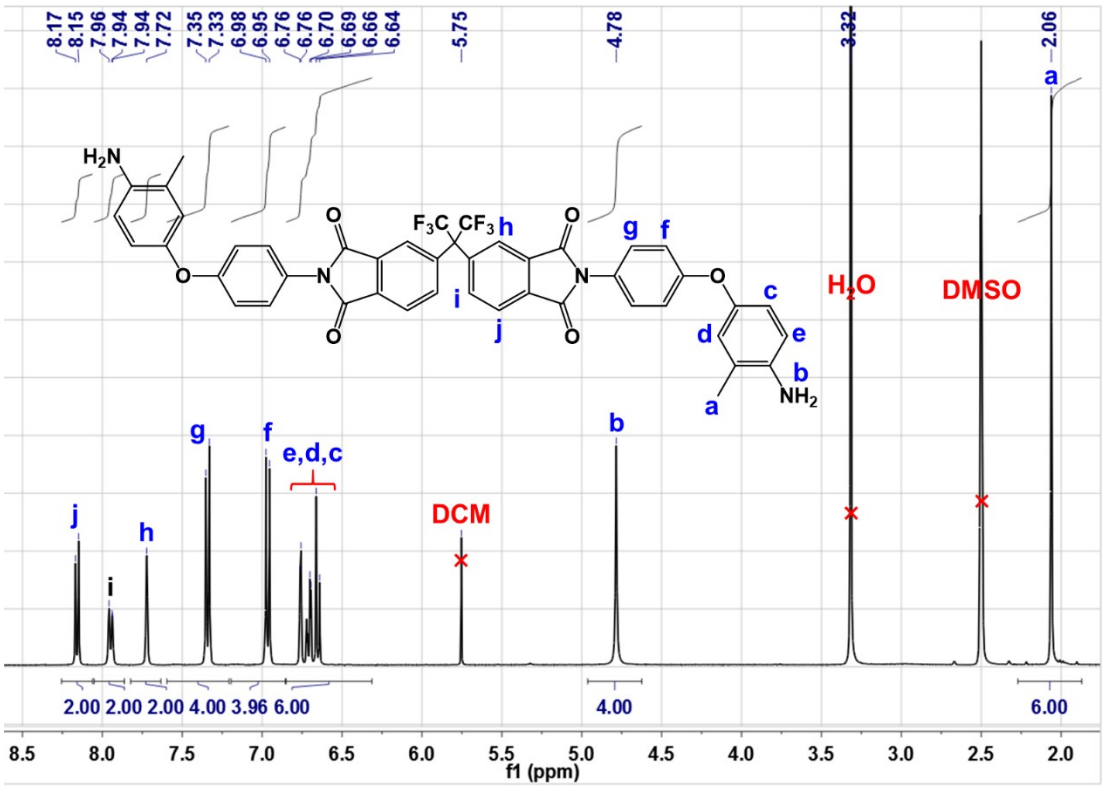

Figure S14. ^{1}H-NMR spectrum of *o*-MBIDA monomer in DMSO-d_6

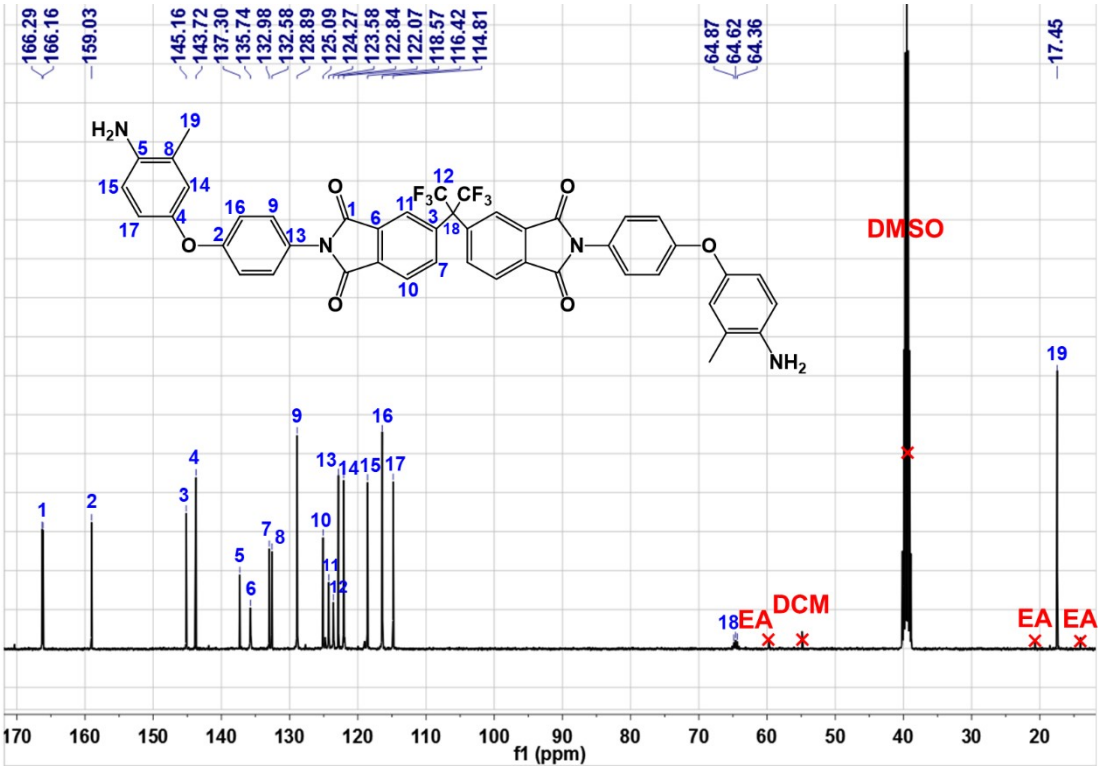

Figure S15. ^{13}C-NMR spectrum of *o*-MBIDA monomer in DMSO-d_6

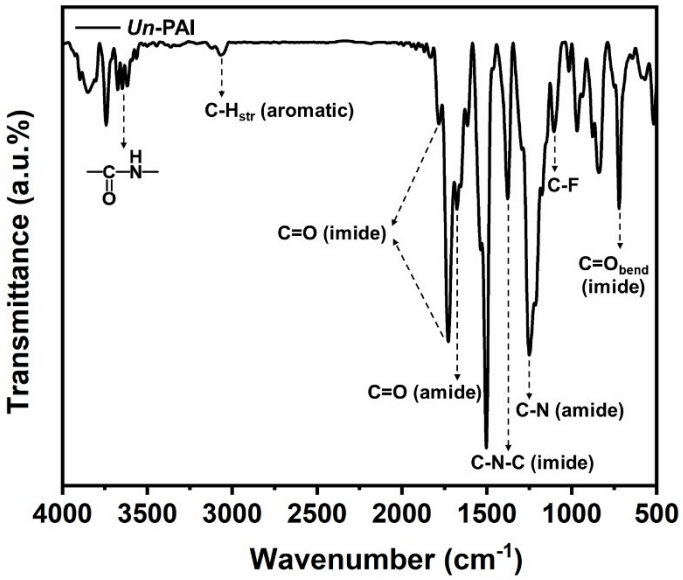

Figure S16. FT-IR spectrum of *Un*-PAI polymer

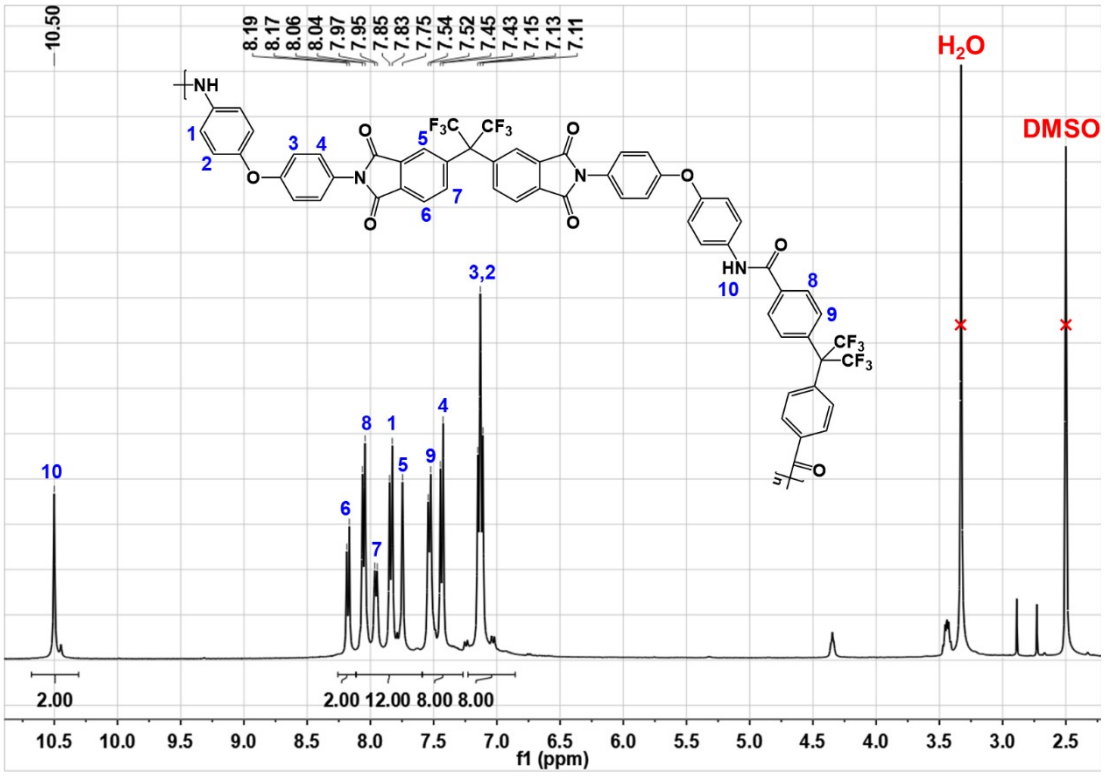

Figure S17. ^{1}H-NMR spectrum of *Un*-PAI polymer in DMSO-d_6

Taking ***Un*-PAI** as an example to analyze the molecular structures of the resulting polymers. As shown in **Figure S17**, the singlet peak locating at ca. 10.5 ppm is attributable to amide hydrogen. The peaks in the range of 8.19-8.17 ppm, 7.97-7.95 ppm and 7.75 ppm are assigned to aromatic protons of **6FDA** moiety, and the peaks at around 7.85-7.83 ppm, 7.45-7.43 ppm and 7.15-7.11 ppm are ascribed to the aromatic hydrogens of **ODA** moiety, while the peaks in the range of 8.06-8.04 ppm and 7.54-7.52 ppm correspond to **6FBA** unit. No signals belonging to primary amine and carboxyl groups can be found, indicating the complete polycondensation of **BIDA** and **6FBA**.

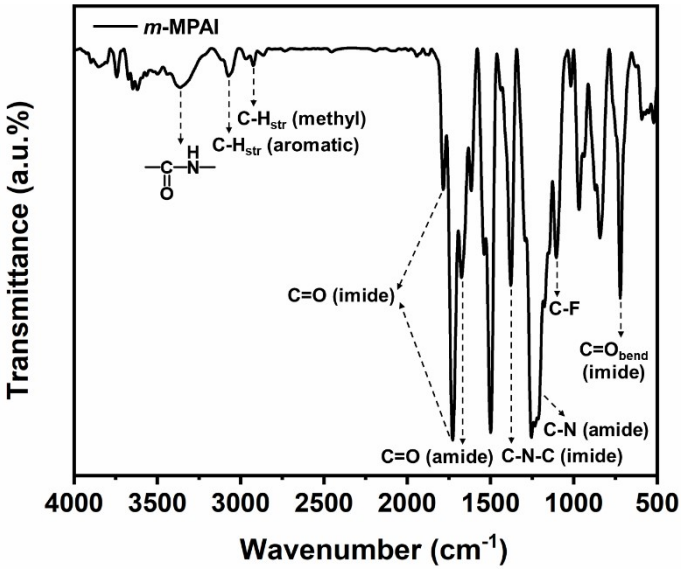

Figure S18. FT-IR spectrum of *m*-MPAI polymer

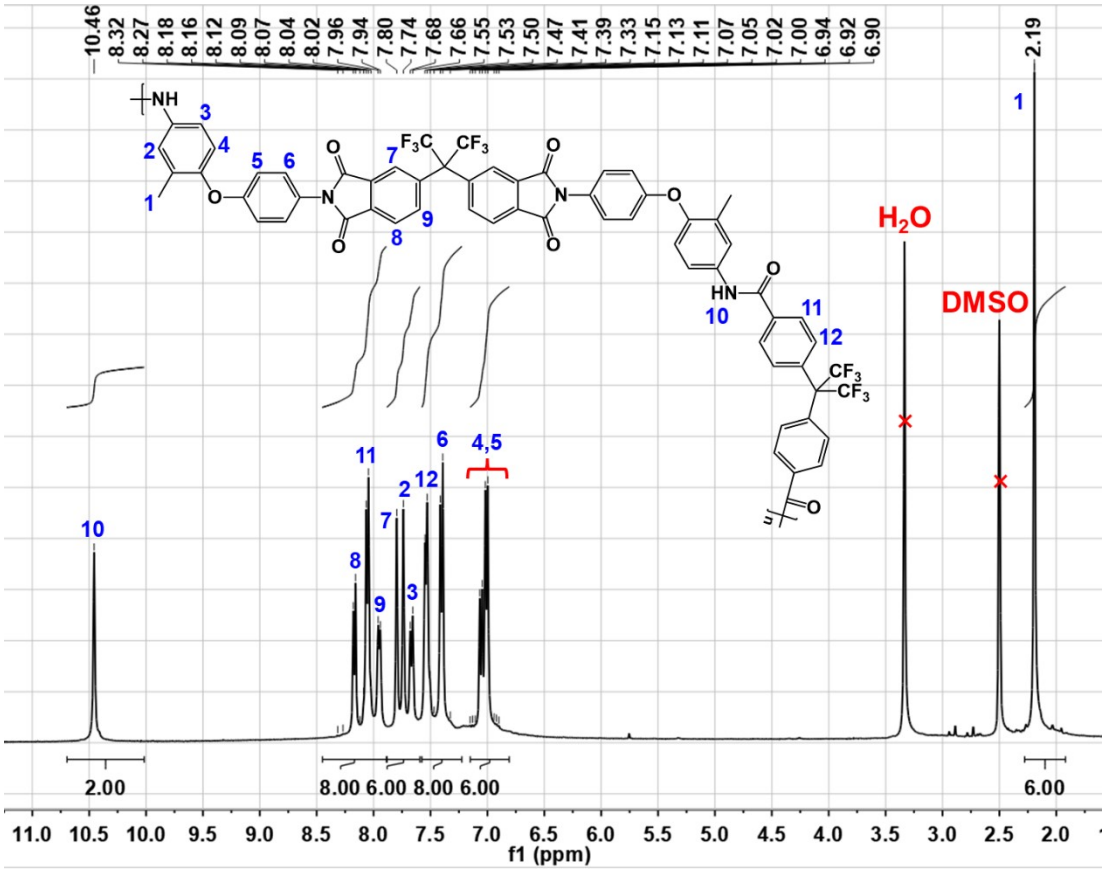

Figure S19. ^{1}H-NMR spectrum of *m*-MPAI polymer in DMSO-d_6

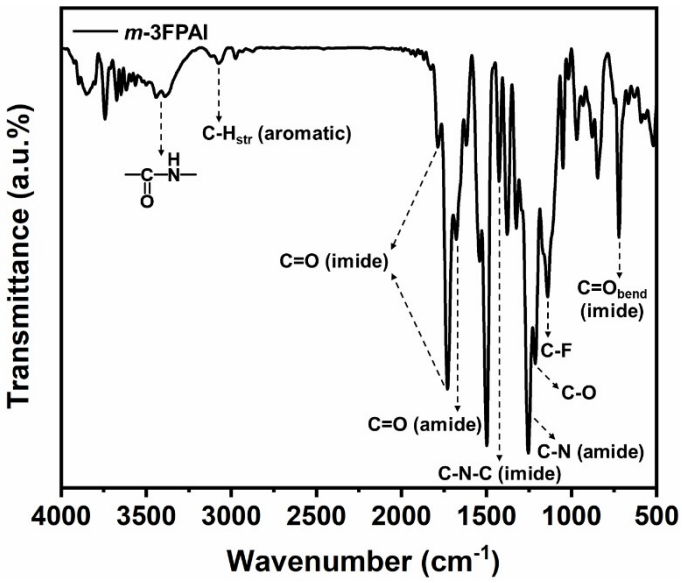

Figure S20. FT-IR spectrum of *m*-3FPAI polymer

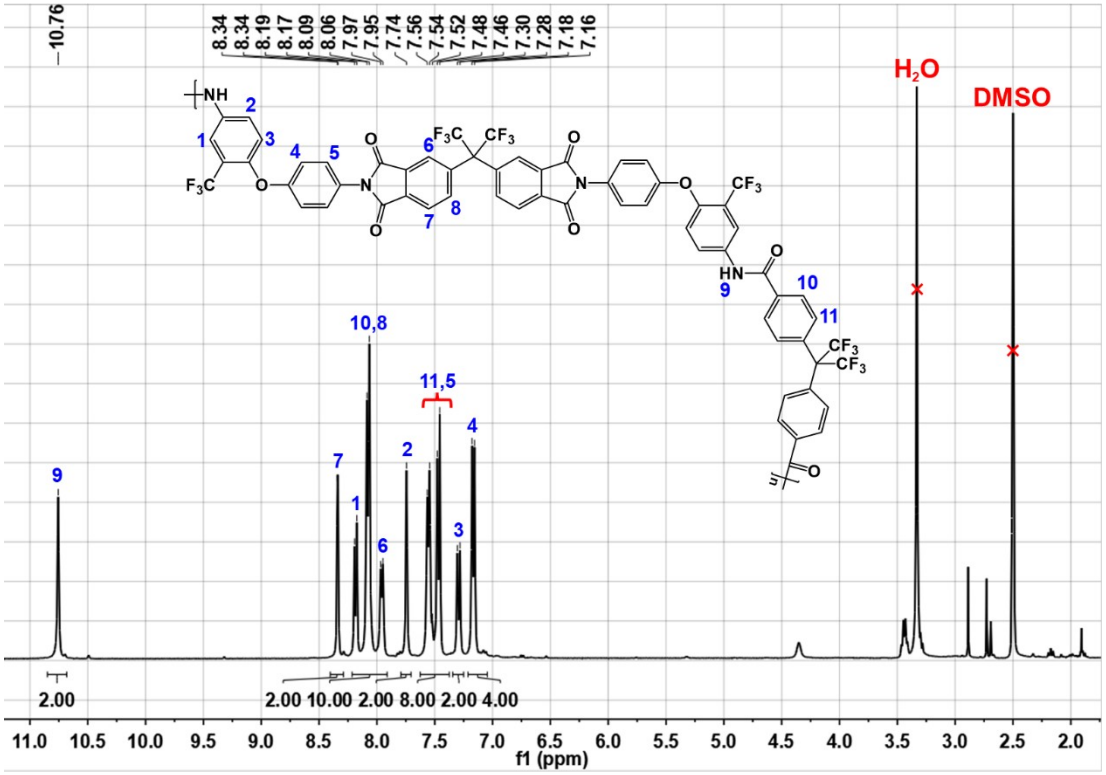

Figure S21. ^{1}H-NMR spectrum of *m*-MPAI polymer in DMSO-d_6

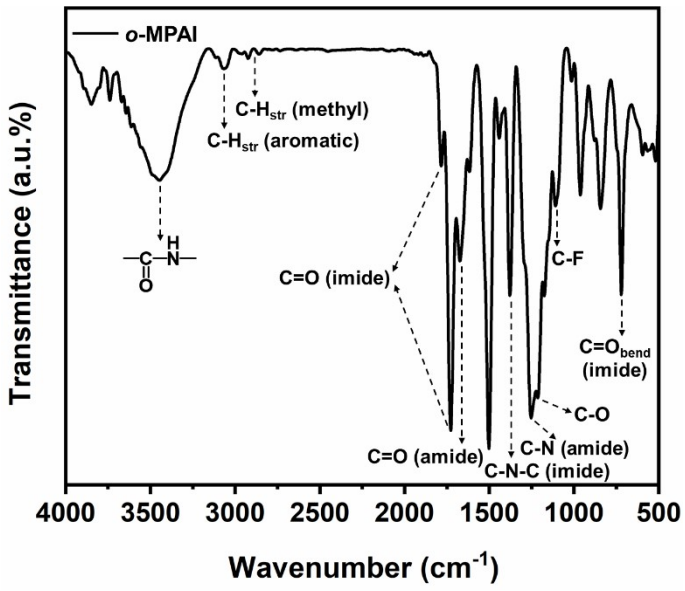

Figure S22. FT-IR spectrum of *o*-MPAI polymer

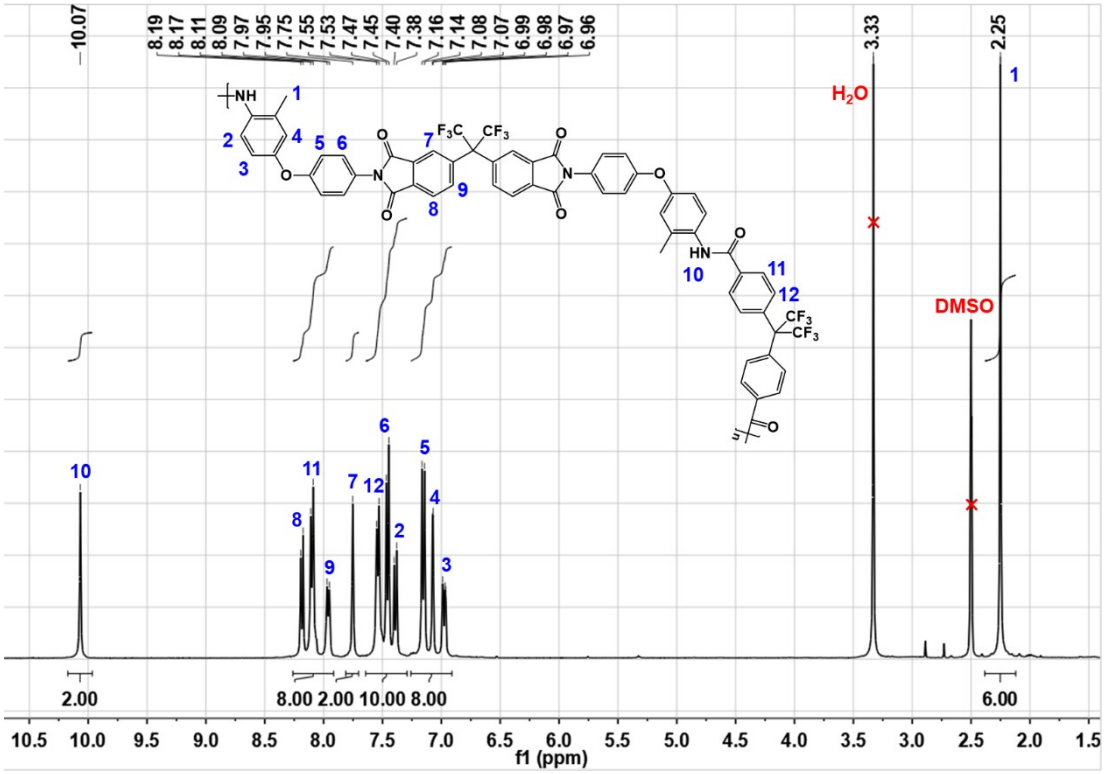

Figure S23. ^{1}H-NMR spectrum of *o*-MPAI polymer in DMSO-d_6

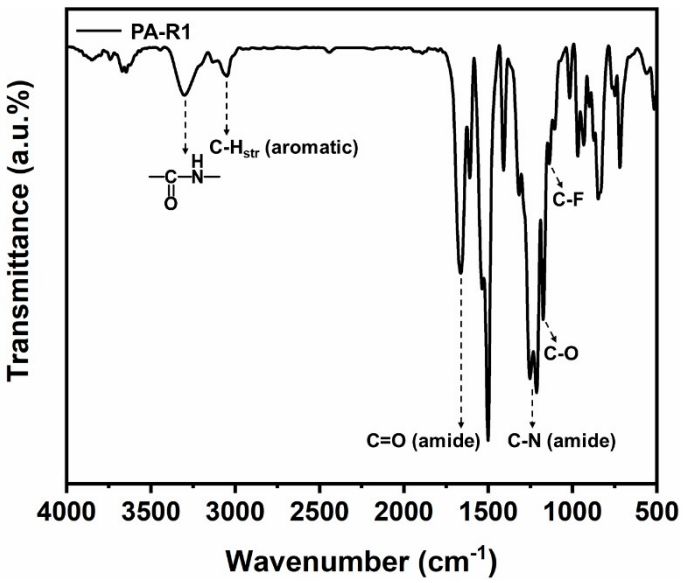

Figure S24. FT-IR spectrum of PA-R1 polymer

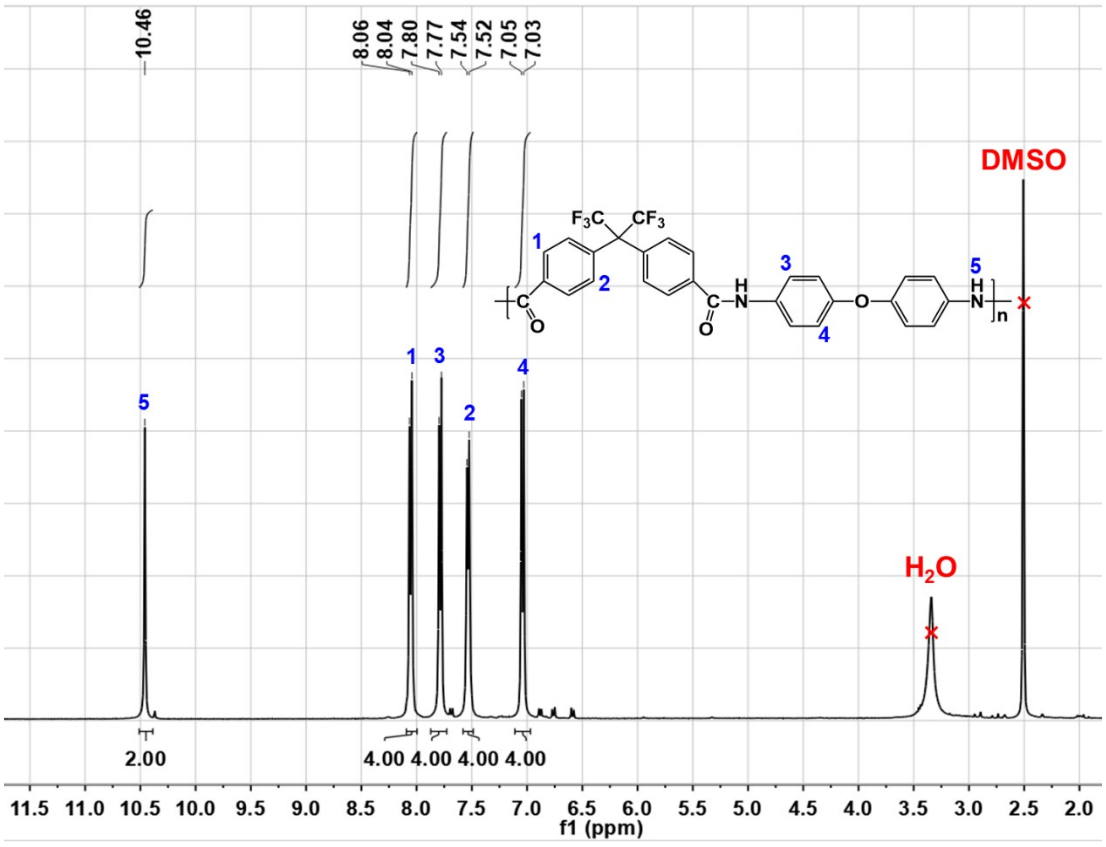

Figure S25. ^{1}H-NMR spectrum of PA-R1 polymer in DMSO-d_6

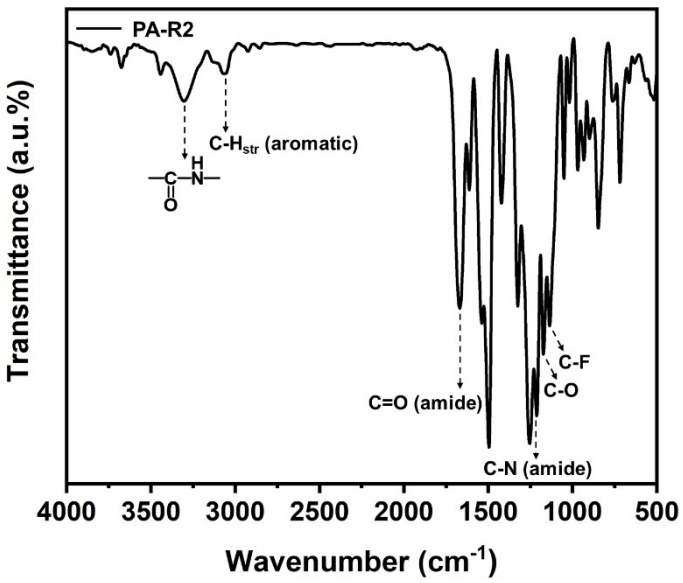

Figure S26. FT-IR spectrum of PA-R2 polymer

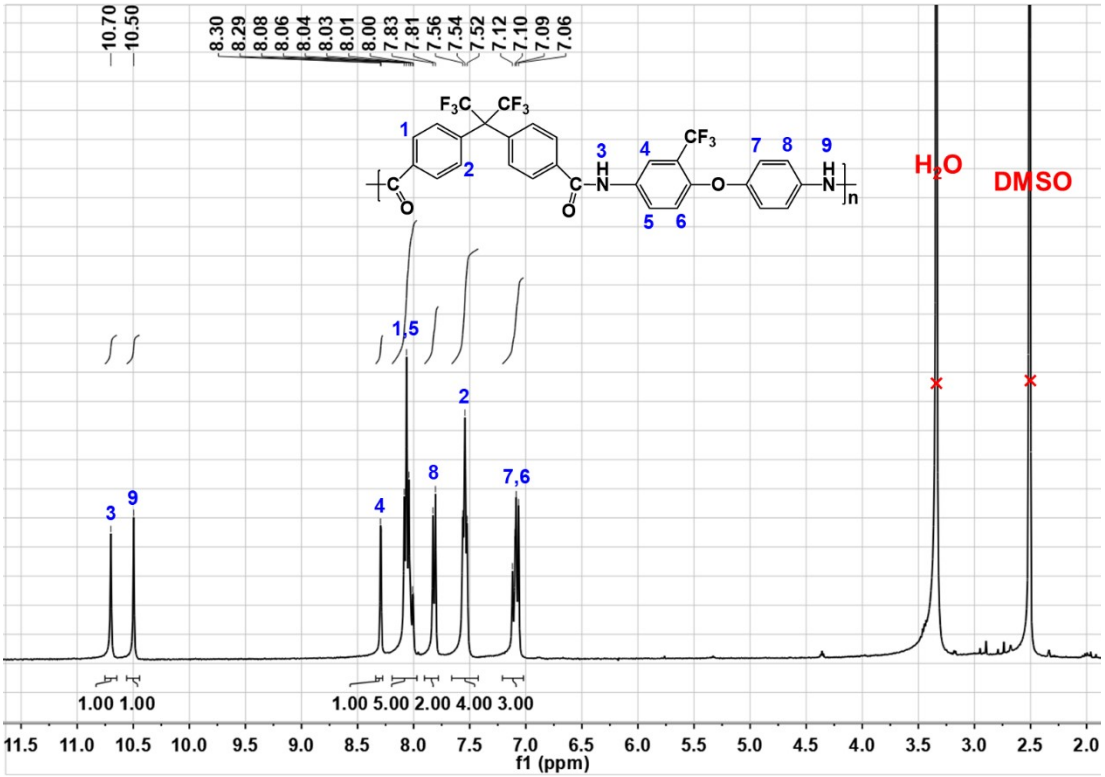

Figure S27. ^{1}H-NMR spectrum of PA-R2 polymer in DMSO-d_6

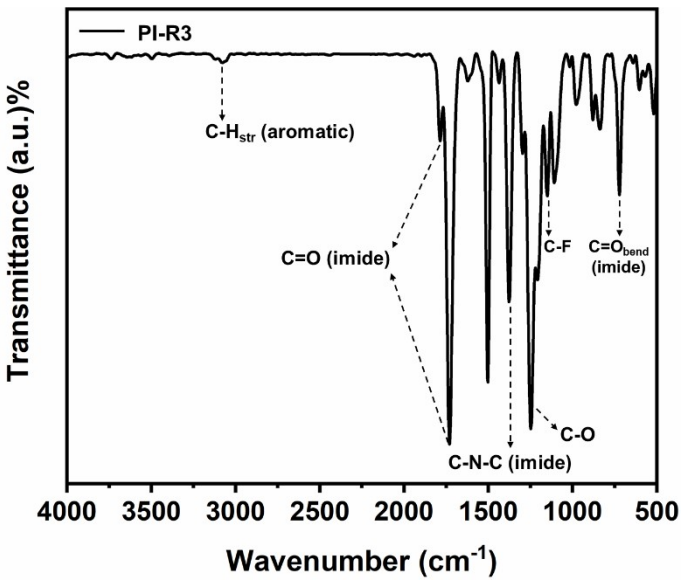

Figure S28. FT-IR spectrum of PI-R3 polymer

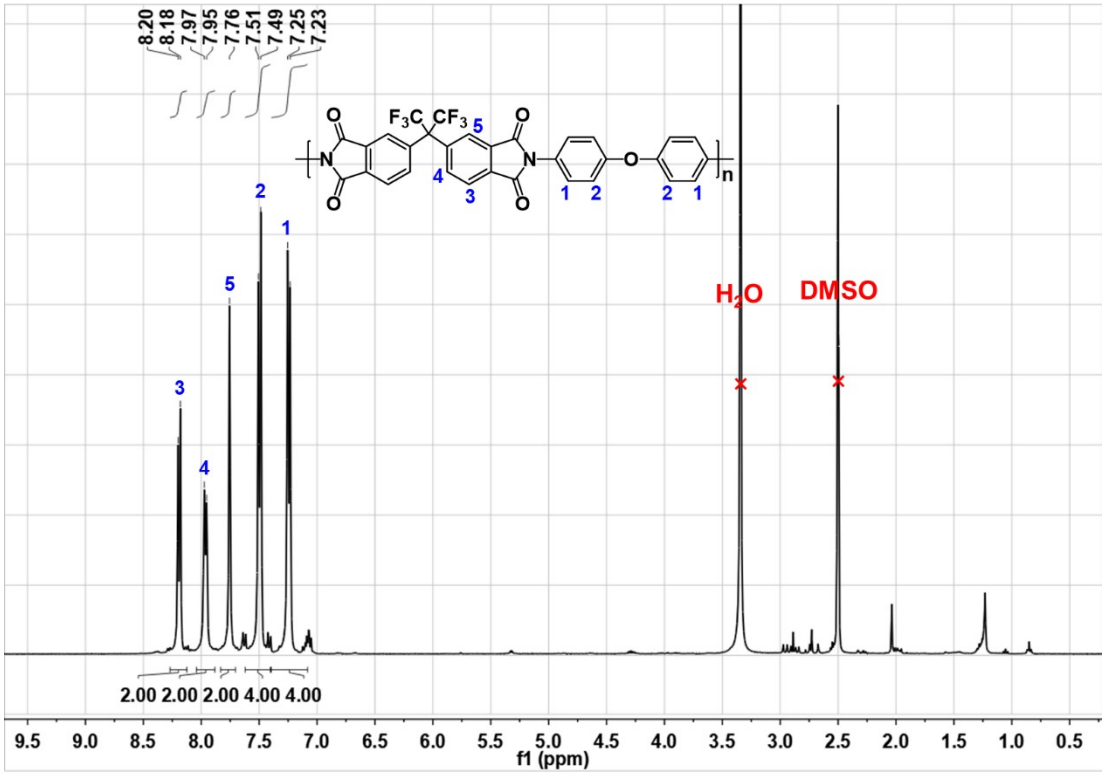

Figure S29. ^{1}H-NMR spectrum of PI-R3 polymer in DMSO-d_6

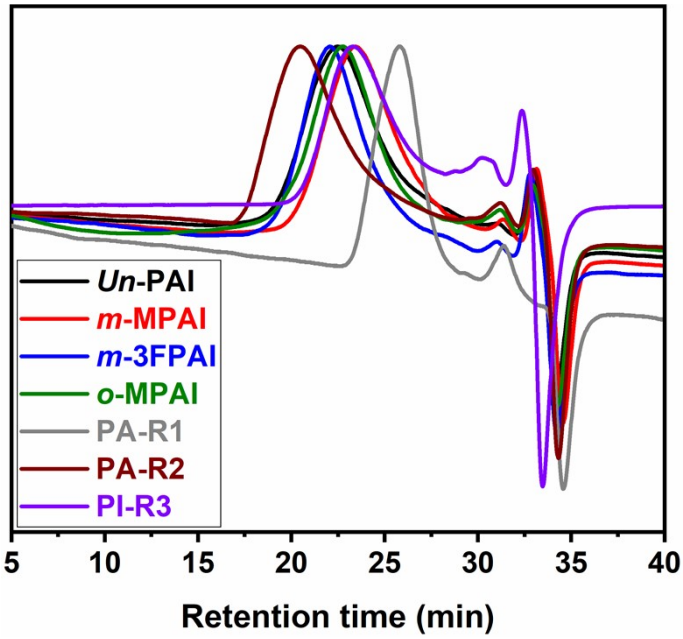

Figure S30. GPC curves of the resulting polymers in THF at 25 °C

Table S1. Organo solubility of the resulting polymers[a]

Samples	DMAc	DMF	NMP	$CHCl_3$	CH_2Cl_2	THF
***Un*-PAI**	+ +	+ +	+ +	+ +	+ –	+ +
***m*-MPAI**	+ +	+ +	+ +	+ +	+ –	+ +
***m*-3FPAI**	+ +	+ +	+ +	+ +	+ +	+ +
***o*-MPAI**	+ +	+ +	+ +	+ +	+ –	+ +
PA-R1	+ –	+ –	+ –	+ –	– –	+ –
PA-R2	+ +	+ +	+ +	+ +	+ –	+ +

[a]+ +: Soluble at room temperature; + –: Partially soluble; – –: Insoluble. DMAc: *N*,*N*-dimethylacetamide, DMF: *N*,*N*-dimethylformamide, NMP: *N*-methylpyrrolidone, THF: tetrahydrofuran.

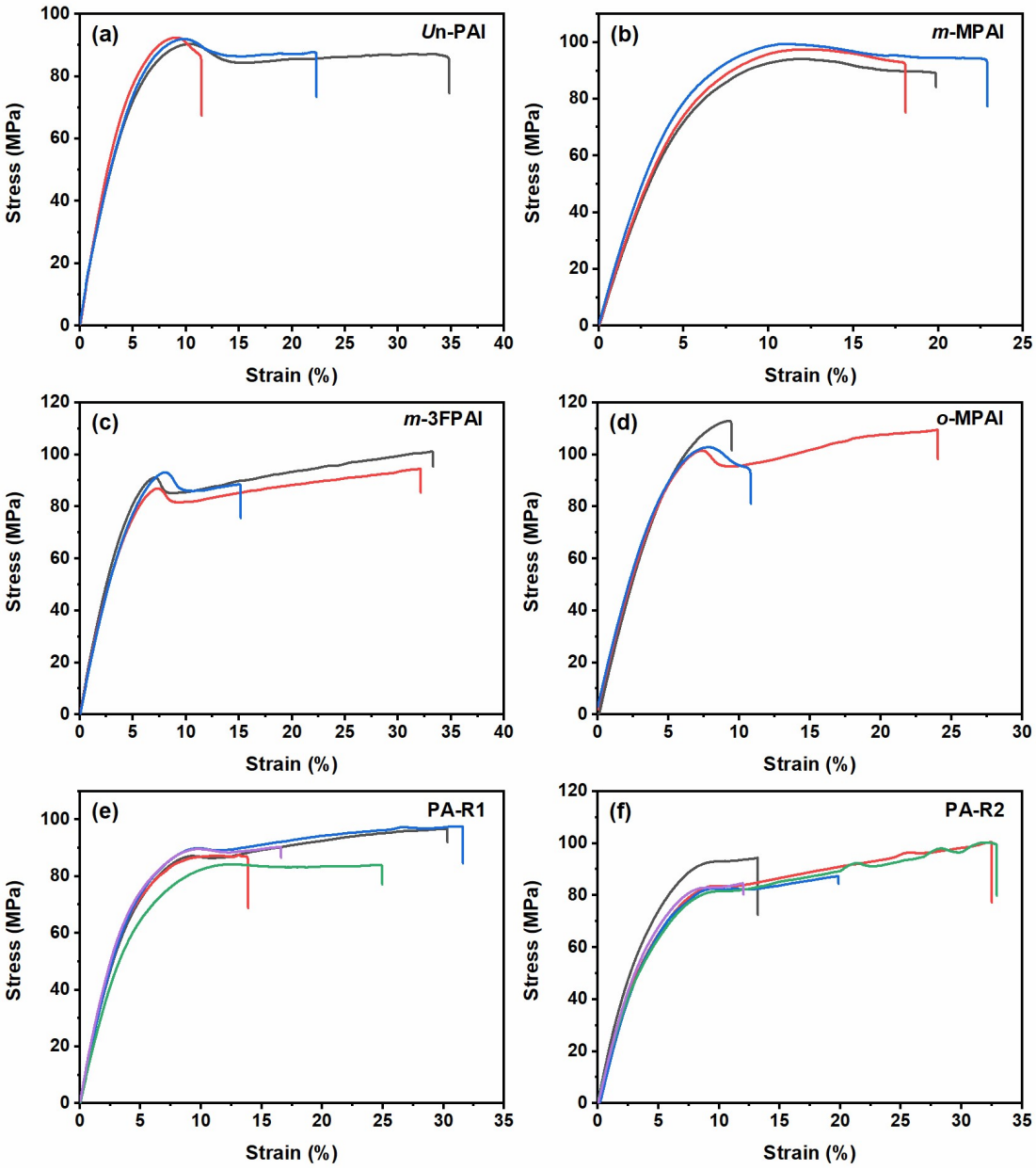

Figure S31. Tensile stress-strain curves of the resulting polymer thin films (dry state) at room temperature: (a) *Un*-PAI, (b) *m*-MPAI, (c) *m*-3FPAI, (d) *o*-MPAI, (e) PA-R1 and (f) PA-R2

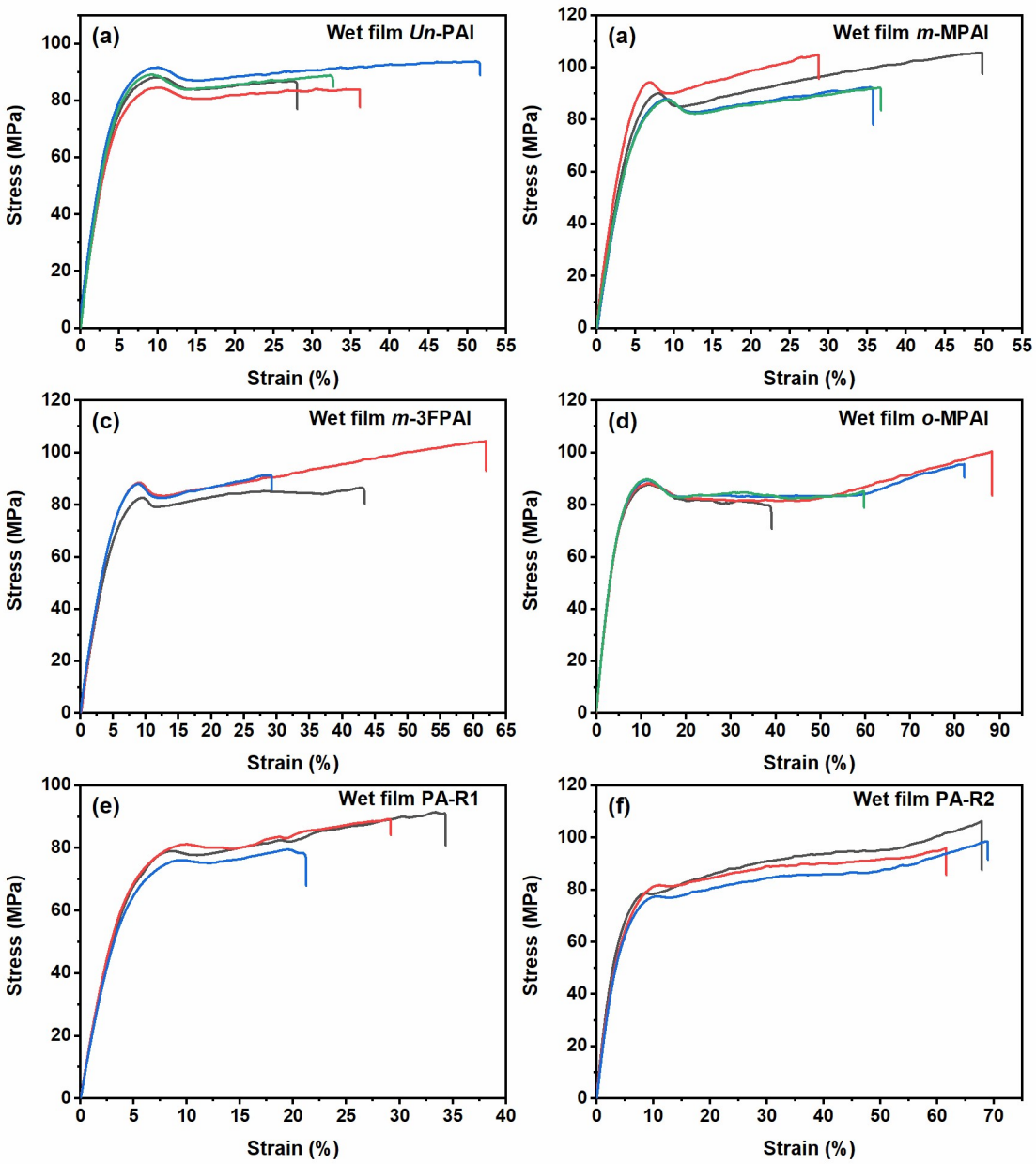

Figure S32. Tensile stress-strain curves of the resulting polymer thin films (wet state) at room temperature: (a) *Un*-PAI, (b) *m*-MPAI, (c) *m*-3FPAI, (d) *o*-MPAI, (e) PA-R1 and (f) PA-R2.

Table S2. Tensile data for wet *Un*-PAI thin films

***Un*-PAI**	**Tensile strength (MPa)**	**Tensile modulus (GPa)**	**Break elongation (%)**	**Fracture toughness ($MJ \cdot m^{-3}$)**
Sample 1	88.1	2.12	28.0	21.9
Sample 2	84.4	2.08	36.1	27.8
Sample 3	93.7	2.24	51.7	44.6
Sample 4	89.0	2.26	32.7	26.1
Average value	88.8	2.17	37.1	30.1
Standard deviation	3.8	0.09	10.3	10.0

Table S3. Tensile data for wet *m*-MPAI thin films

***m*-MPAI**	**Tensile strength (MPa)**	**Tensile modulus (GPa)**	**Break elongation (%)**	**Fracture toughness ($MJ \cdot m^{-3}$)**
Sample 1	105.7	2.09	49.8	44.9
Sample 2	104.7	2.58	28.7	25.4
Sample 3	92.2	2.00	35.8	28.8
Sample 4	92.1	1.99	36.7	29.5
Average value	98.7	2.17	37.8	32.2
Standard deviation	7.6	0.28	8.8	8.7

Table S4. Tensile data for wet *m*-3FPAI thin films

***m*-3FPAI**	**Tensile strength (MPa)**	**Tensile modulus (GPa)**	**Break elongation (%)**	**Fracture toughness ($MJ \cdot m^{-3}$)**
Sample 1	86.5	1.78	43.5	33.6
Sample 2	104.3	1.90	62.0	54.9
Sample 3	91.3	1.93	29.2	22.8
Average value	94.1	1.87	44.9	37.1
Standard deviation	9.2	0.08	16.5	16.3

Table S5. Tensile data for wet *o*-MPAI thin films

***o*-MPAI**	**Tensile strength (MPa)**	**Tensile modulus (GPa)**	**Break elongation (%)**	**Fracture toughness ($MJ \cdot m^{-3}$)**
Sample 1	100.4	1.95	88.3	74.2
Sample 2	95.5	1.83	82.1	68.0
Sample 3	89.7	1.89	59.7	47.9

Sample 4	87.7	1.90	39.1	30.0
Average value	93.3	1.89	67.3	55.1
Standard deviation	5.8	0.05	22.5	20.1

Table S6. Tensile data for wet PA-R1 thin films

PA-R1	Tensile strength (MPa)	Tensile modulus (GPa)	Break elongation (%)	Fracture toughness ($MJ \cdot m^{-3}$)
Sample 1	91.5	1.98	34.3	26.4
Sample 2	89.2	1.97	29.2	22.0
Sample 3	79.5	1.93	21.3	14.2
Average value	86.7	1.96	28.3	20.9
Standard deviation	6.4	0.03	6.6	6.1

Table S7. Tensile data for wet PA-R2 thin films

PA-R2	Tensile strength (MPa)	Tensile modulus (GPa)	Break elongation (%)	Fracture toughness ($MJ \cdot m^{-3}$)
Sample 1	106.4	2.03	67.9	59.4
Sample 2	96.0	1.84	61.6	51.4
Sample 3	98.5	1.84	69.0	56.2
Average value	100.3	1.904	66.2	55.7
Standard deviation	5.4	0.11	4.0	4.1

Table S8. Six consecutive shape memory properties for *m*-3FPAI thin films

Round	ε_s (%)	ε_m (%)	ε_u (%)	ε_p (%)	R_f (%)	R_r (%)
1	6.75	44.40	43.89	6.23	98.6	100
2	5.88	46.07	45.49	6.36	98.6	98.8
3	5.47	48.09	47.43	6.41	98.5	97.8
4	5.86	49.89	49.22	6.16	98.5	99.3
5	6.60	51.52	50.84	6.71	98.5	99.8
6	5.61	53.07	52.37	5.92	98.5	99.3

Table S9. Storage modulus of the resulting polymers at different temperature

Samples	*E*' (50 °C) GPa	*E*' (T_g-50 °C) GPa	*E*' (T_g+10 °C) MPa	*E*' (T_g-50 °C)/*E*' (T_g+10 °C)
***Un*-PAI**	1.89	0.98	11.5	85.2
***m*-MPAI**	2.76	1.46	17.8	82.0

***m*-3FPAI**	2.51	1.29	11.4	113.2
***o*-MPAI**	2.27	1.49	17.3	86.1
PA-R1	2.34	1.42	14.7	96.6
PA-R2	2.15	1.27	16.0	79.4
PI-R3	2.72	1.27	25.9	49.0

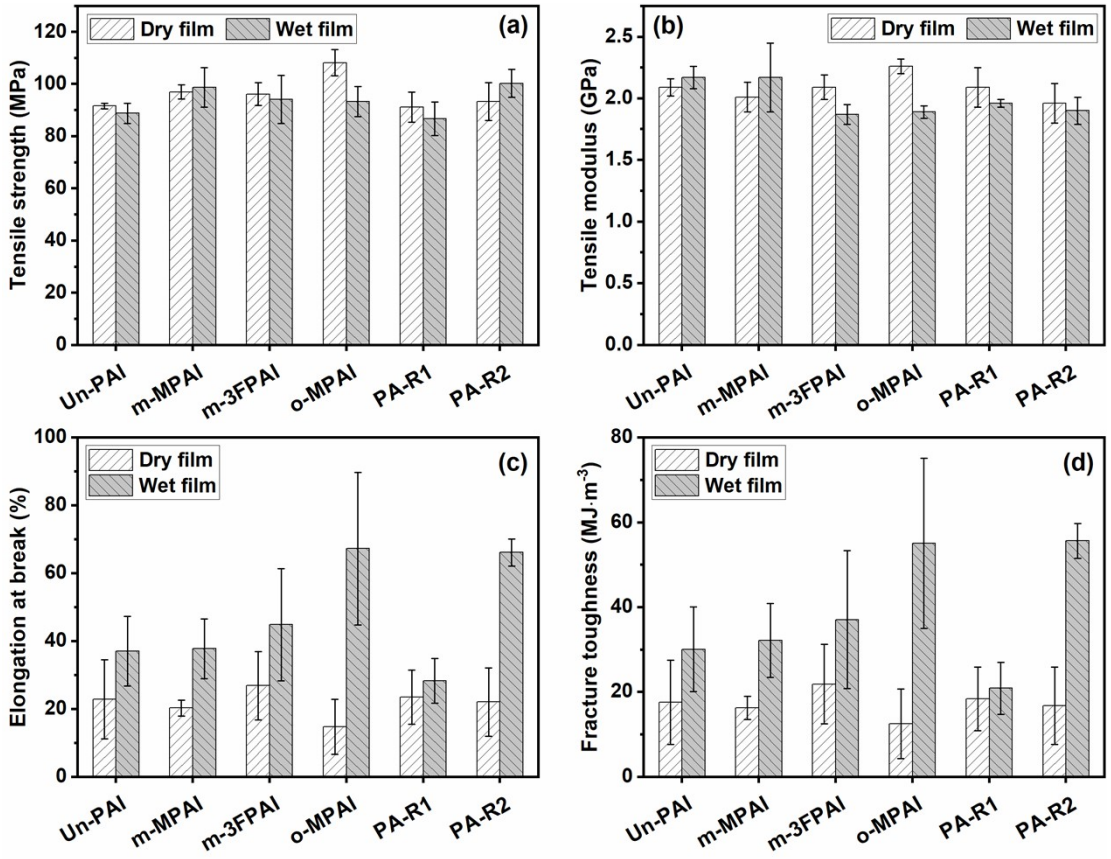

Figure S33. Mechanical properties of the resulting polymer thin films in dry and wet states: (a) tensile strength, (b) tensile modulus, (c) elongation at break, (d) fracture toughness.

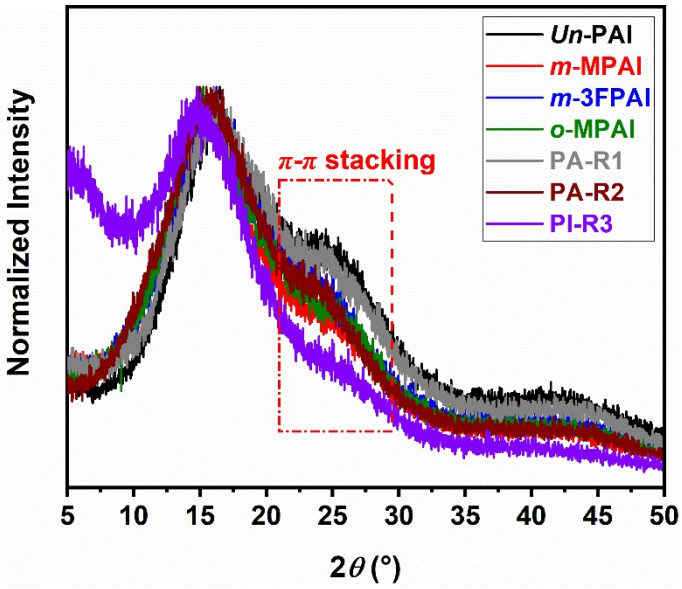

Figure S34. WAXD patterns of the resulting polymers.

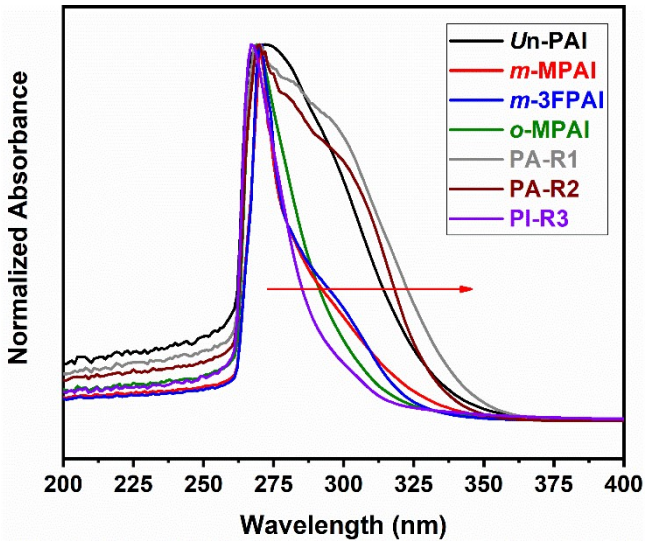

Figure S35. UV absorption spectra of the resulting polymers.

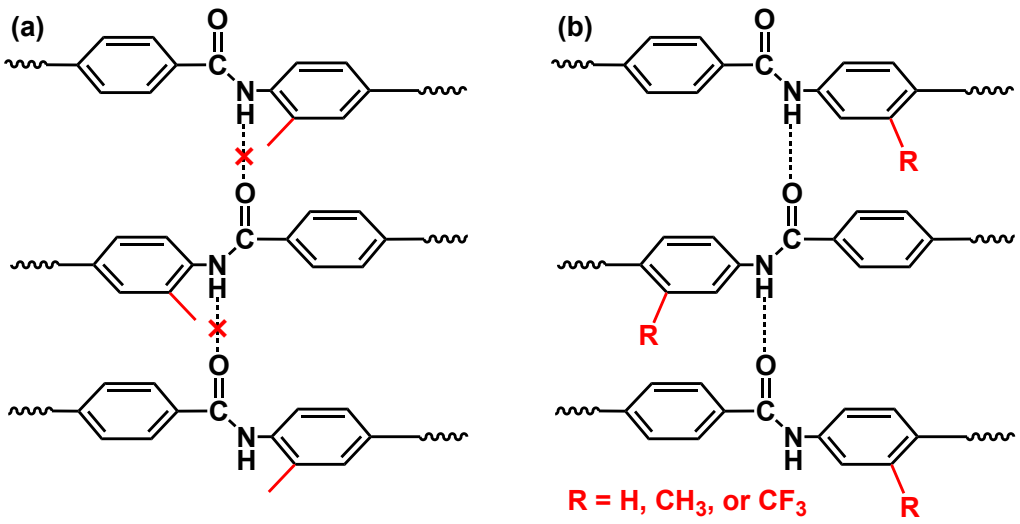

Figure S36. Proposed formation of hydrogen bonding interaction within (a) *o*-MPAI and (b) *Un*-PAI, *m*-MPAI and *m*-3FPAI polymer networks.

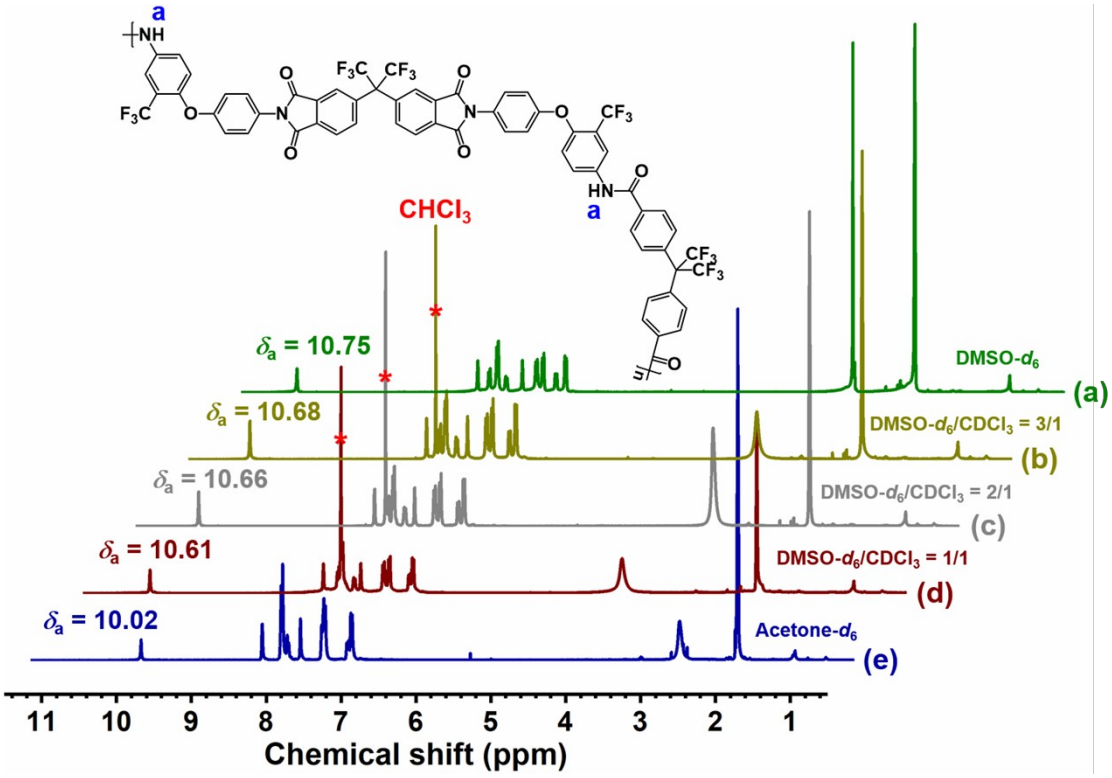

Figure S37. Demonstration of H-bond formation between *m*-3FPAI main chains. ^{1}H-NMR spectra of *m*-3FPAI polymer at room temperature in (a) DMSO-d_6, (b) DMSO-d_6/$CDCl_3$ (v/v = 3/1), (c) DMSO-d_6/$CDCl_3$ (v/v = 2/1), (d) DMSO-d_6/$CDCl_3$ (v/v = 1/1), (e) acetone-d_6 (concentration: 10 mg·mL^{-1}). *indicates $CHCl_3$ signal.

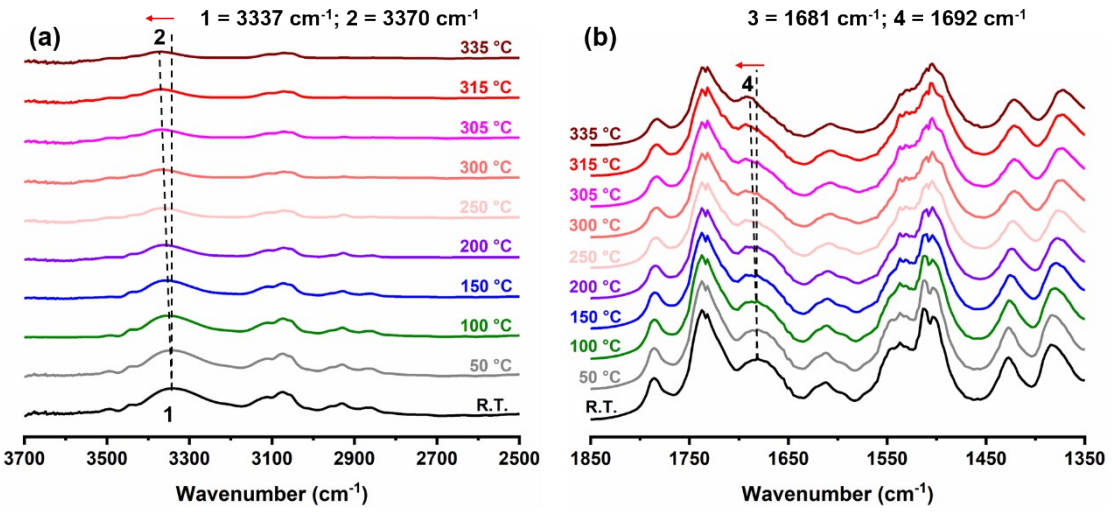

Figure S38. Variable temperature IR spectra of *m*-3FPAI: (a) expanded amide N-H stretching region from 2500 cm^{-1} to 3700 cm^{-1} and (b) enlarged amide carbonyl stretching region from 1350 cm^{-1} to 1850 cm^{-1}.

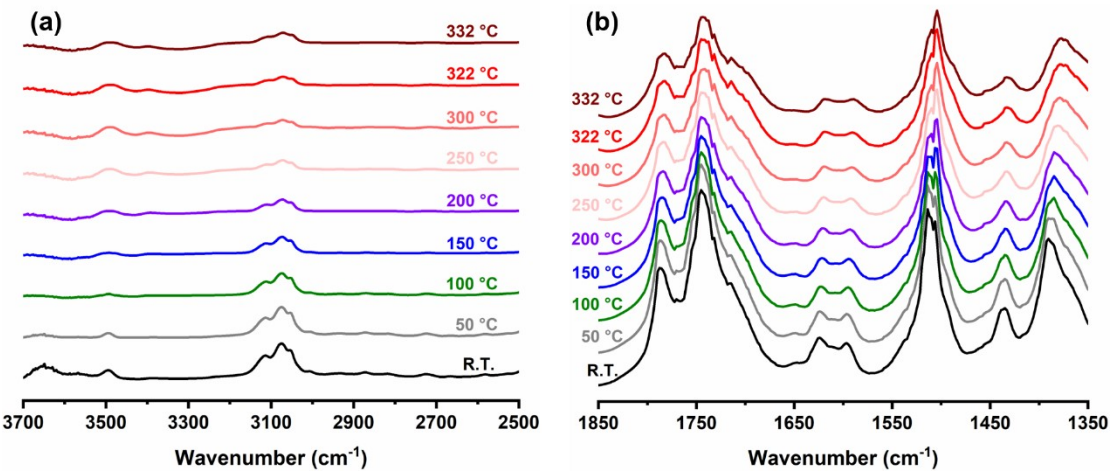

Figure S39. Variable temperature IR spectra of reference PI-R3: (a) expanded region from 2500 cm^{-1} to 3700 cm^{-1} and (b) enlarged imide carbonyl stretching region from 1350 cm^{-1} to 1850 cm^{-1}.

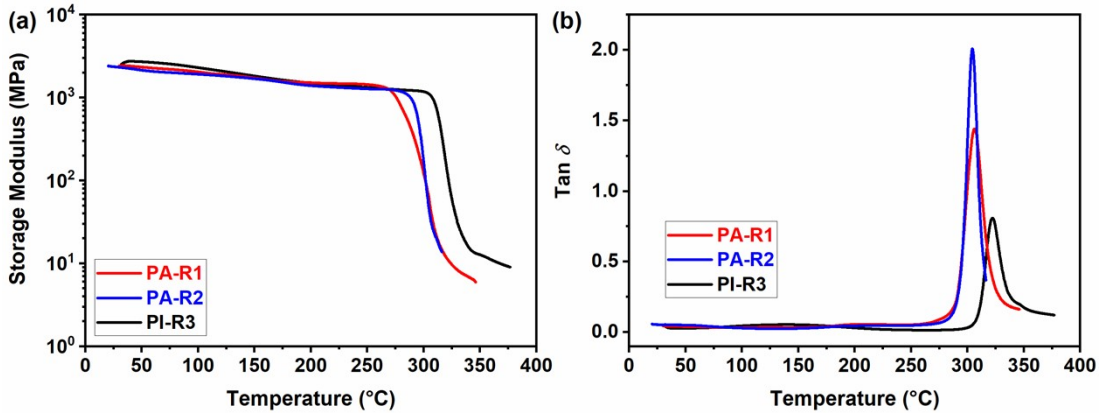

Figure S40. Thermal dynamic traces of the reference samples for PA-R1, PA-R2 and PI-R3: (a) storage modulus curves and (b) tan δ curves.

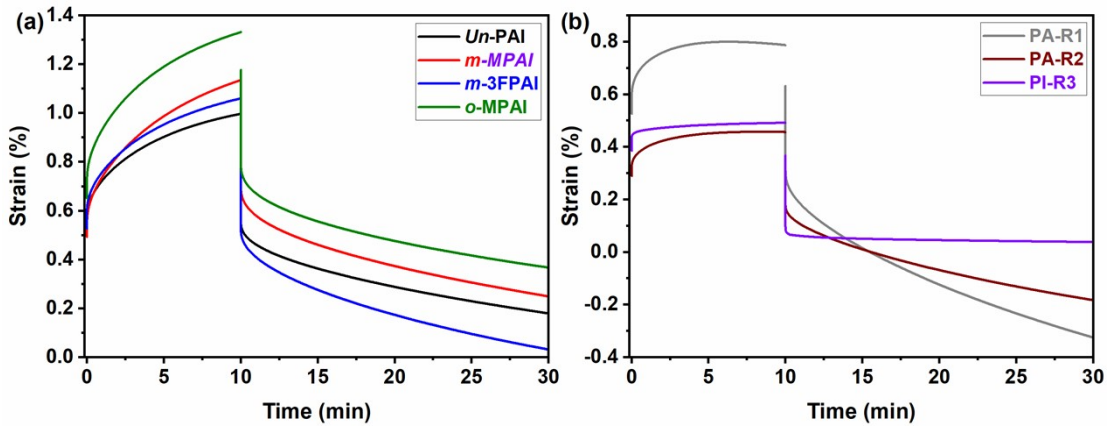

Figure S41. Creep recovery curves of the resulting polymers measured at 180 °C under 5 MPa load.

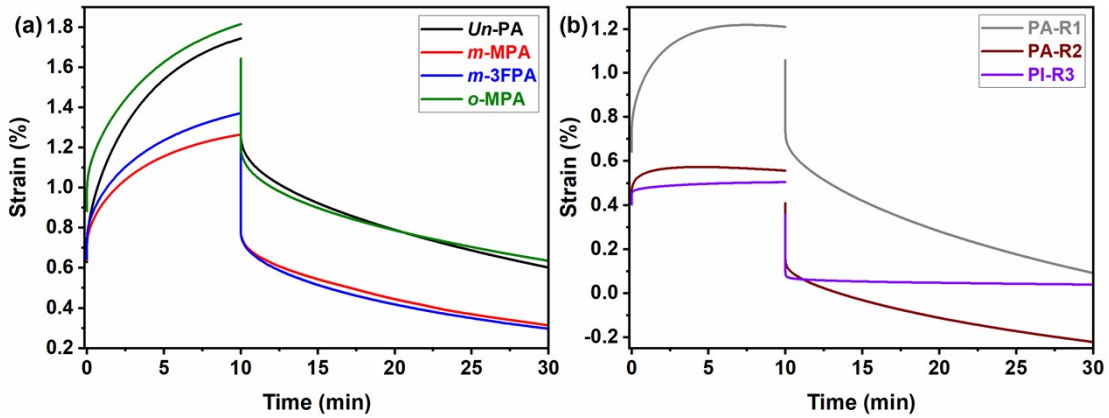

Figure S42. Creep recovery curves of the resulting polymers measured at 200 °C under 5 MPa load.

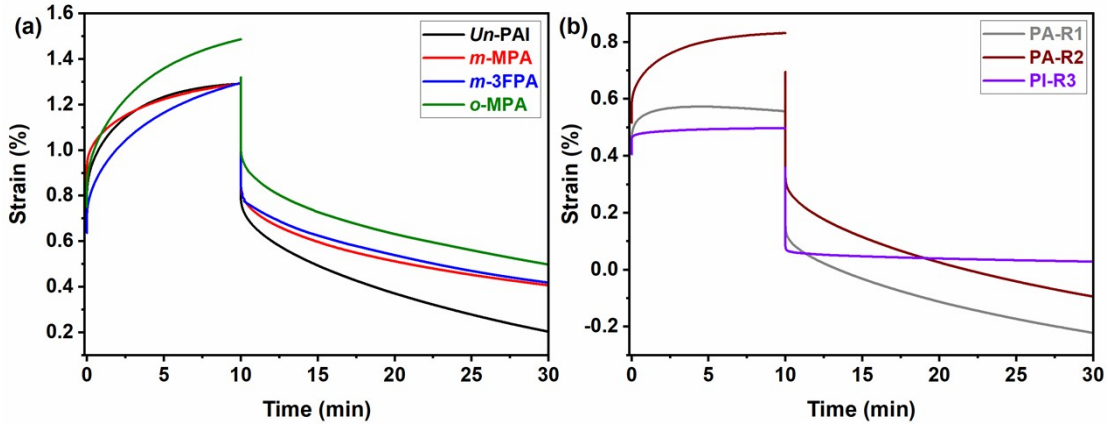

Figure S43. Creep recovery curves of the resulting polymers measured at 220 °C under

5 MPa load.

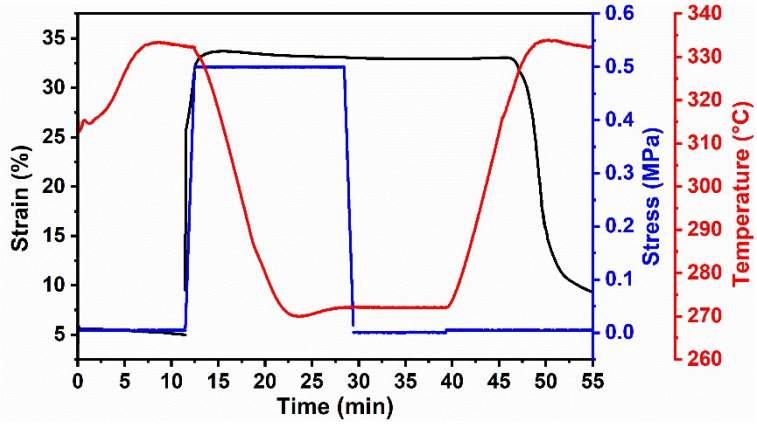

Figure S44. Thermal-triggered dual-shape memory behavior of PI-R3.

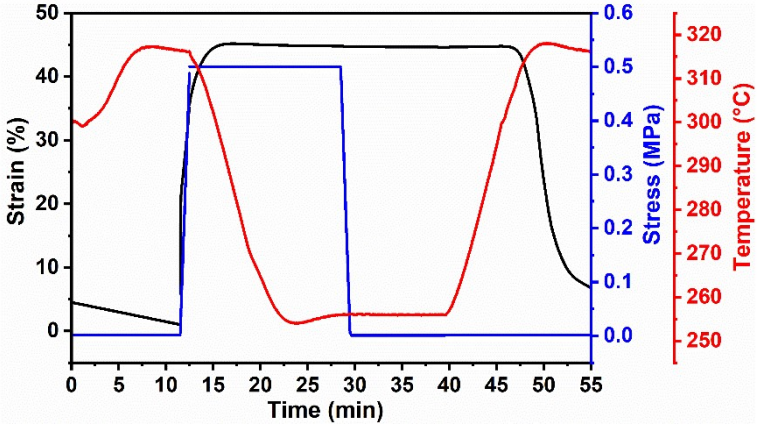

Figure S45. Thermal-triggered dual-shape memory behavior of PA-R1.

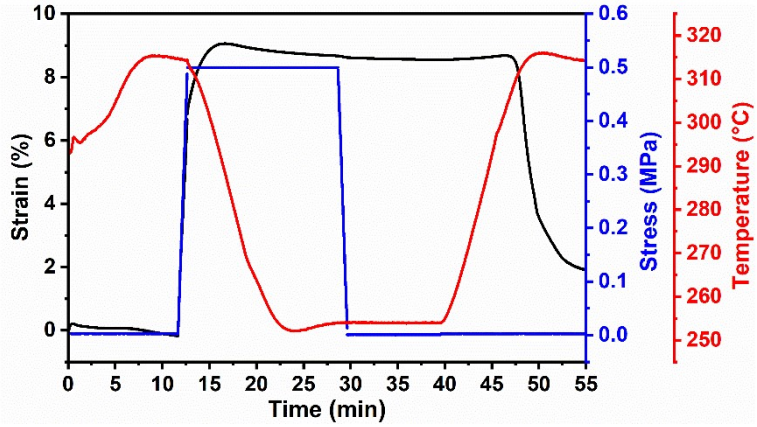

Figure S46. Thermal-triggered dual-shape memory behavior of PA-R2.

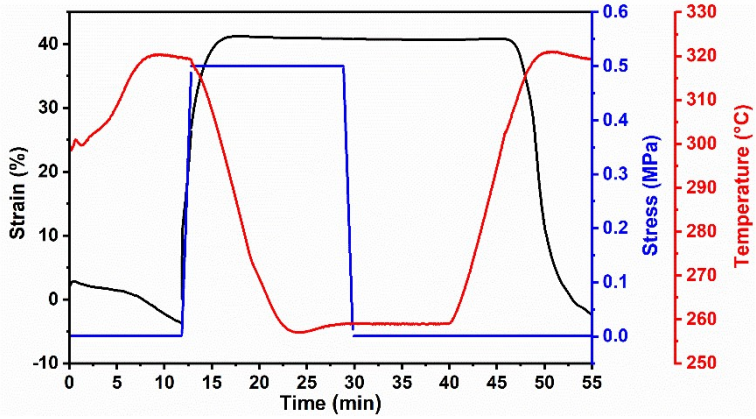

Figure S47. Thermal-triggered dual-shape memory behavior of *Un*-PAI.

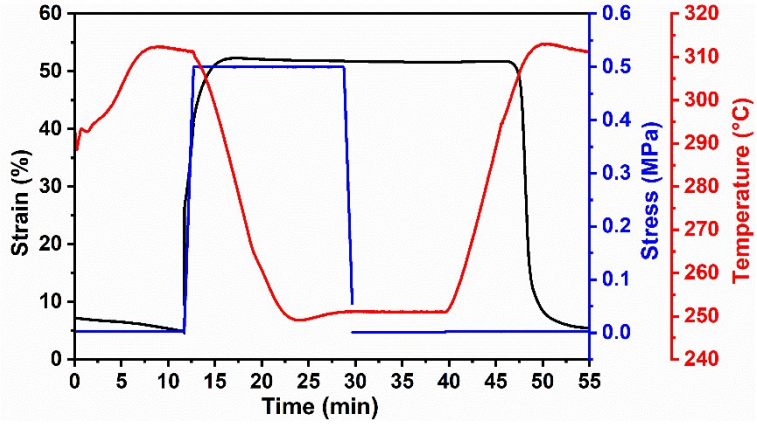

Figure S48. Thermal-triggered dual-shape memory behavior of *m*-MPAI.

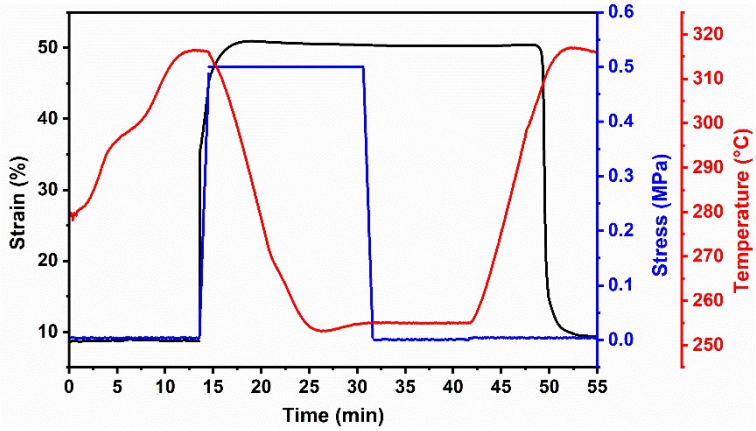

Figure S49. Thermal-triggered dual-shape memory behavior of *m*-3FPAI.

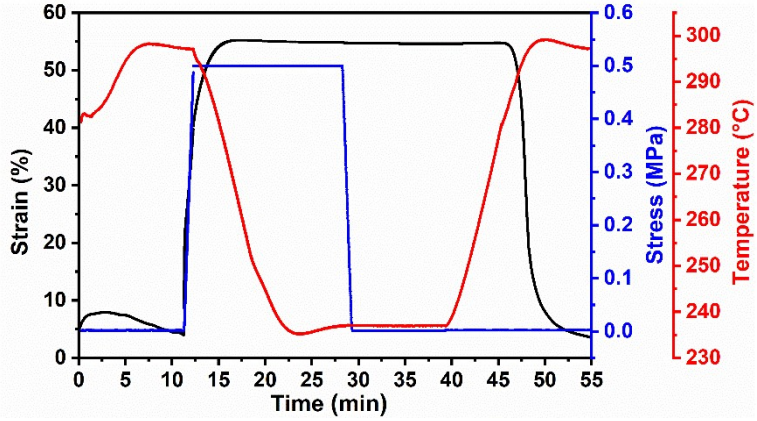

Figure S50. Thermal-triggered dual-shape memory behavior of *o*-MPAI.